Fine-scale rainfall over New Caledonia under climate change

Cyril Dutheil, Christophe E. Menkès, Matthieu Lengaigne, Jérôme Vialard, Alexandre Peltier, Margot Bador, X. Petit

HAL Id: hal-02975582

https://hal.sorbonne-universite.fr/hal-02975582

Submitted on 22 Oct 2020

Fine-scale rainfall over New Caledonia under climate change

Cyril Dutheil[1,2,3] · C. Menkes[2] · M. Lengaigne[4] · J. Vialard[4] · A. Peltier[5] · M. Bador[6] · X. Petit[1]

Abstract

Global climate models projections indicate no clear future rainfall changes over the Southwestern Pacific islands in response to anthropogenic forcing. Yet, these models have low (~ 100–200 km) spatial resolution and suffer from large systematic biases, such as the trademark "double ITCZ". Here, 4 km-resolution simulations were used with a nested regional atmospheric model, which resolves the New Caledonian mountainous topography. The resulting present-day rainfall amount, spatial structure, seasonal cycle, and extremes compare much better with observations than at 20 km resolution. We applied projected changes from global climate models under the RCP8.5 scenario at the boundaries, following an approach that corrects both their present-day and projected sea surface temperature biases. Unlike climate models, our refined projections reveal an 18% decrease in annual mean rainfall over New Caledonia by 2080–2100, especially on the leeward side of the island (up to 30%) and during the hot season (that accounts for ~ 80% of the rainfall decrease). This drying is robust without bias correction, and much stronger than at ~ 20 km resolution. It is mainly driven by circulation changes. A weather regime classification further demonstrates that ~ 80% of the hot season drying relates to a strong anti-cyclonic and air subsidence anomalies centred on the north of NC, which reduces moisture convergence over the archipelago. The frequency and intensity of extreme precipitation events is also reduced by ~ 20% by 2080–2100. This drastic projected drying would have dramatic impacts on water resources and terrestrial ecosystems, pleading for carefully-planned adaptation policies for New Caledonia.

✉ Cyril Dutheil
cyril.dutheil@io-warnemuende.de

1   IRD (Institut de Recherche Pour Le Développement)-Sorbonne Universités (UPMC, Université Paris 06)-CNRS-MNHN-IPSL, LOCEAN Laboratory, IRD Nouméa BP A5, 98848 Nouméa cedex, New Caledonia

2   IRD, ENTROPIE (UMR 9220), BP A5, 98848 Nouméa cedex, New Caledonia

3   Present Address: Present address: Department of Physical Oceanography and Instrumentation, Leibniz Institute for Baltic Sea Research Warnemünde, Rostock, Germany

4   LOCEAN-IPSL, Sorbonne Universités, UPMC, Université Paris 06, CNRS-IRD-MNHN, Paris, France

5   Météo France, Nouméa, New Caledonia

6   Climate Change Research Centre and ARC Centre of Excellence for Climate Extremes, School of BEES, University of New South Wales, Sydney, NSW, Australia

1 Introduction

The New Caledonia (NC) archipelago is located in the Southwest Pacific about 1500 km to the east of Australia and to the north of New Zealand (Fig. 1a). While the average annual rainfall is high (~ 5 mm.day^{-1}), water is regarded as a vulnerable resource in New Caledonia since ~ 70% of the total rainfall occurs within ~ 15 days (Moron et al. 2016), mainly during the first quarter of the year. Hill reservoirs and dams were built a decade ago to reduce the risks of water (including drinking water) shortages, but are now insufficient to meet the growing needs of various economic sectors, such as agriculture (https://www.forumh2o.nc). The west coast of NC is indeed the only sufficiently flat region for modern agriculture (Bonvallot et al. 2012), but is also the driest one because of its downwind location (Maitrepierre and Caudmont 2007). A decrease in rainfall there would have serious consequences for agriculture. Future changes in water availability are also an issue for the NC unique biodiversity. The NC archipelago is a biodiversity hotspot, both underwater and over land. The NC mainland is surrounded
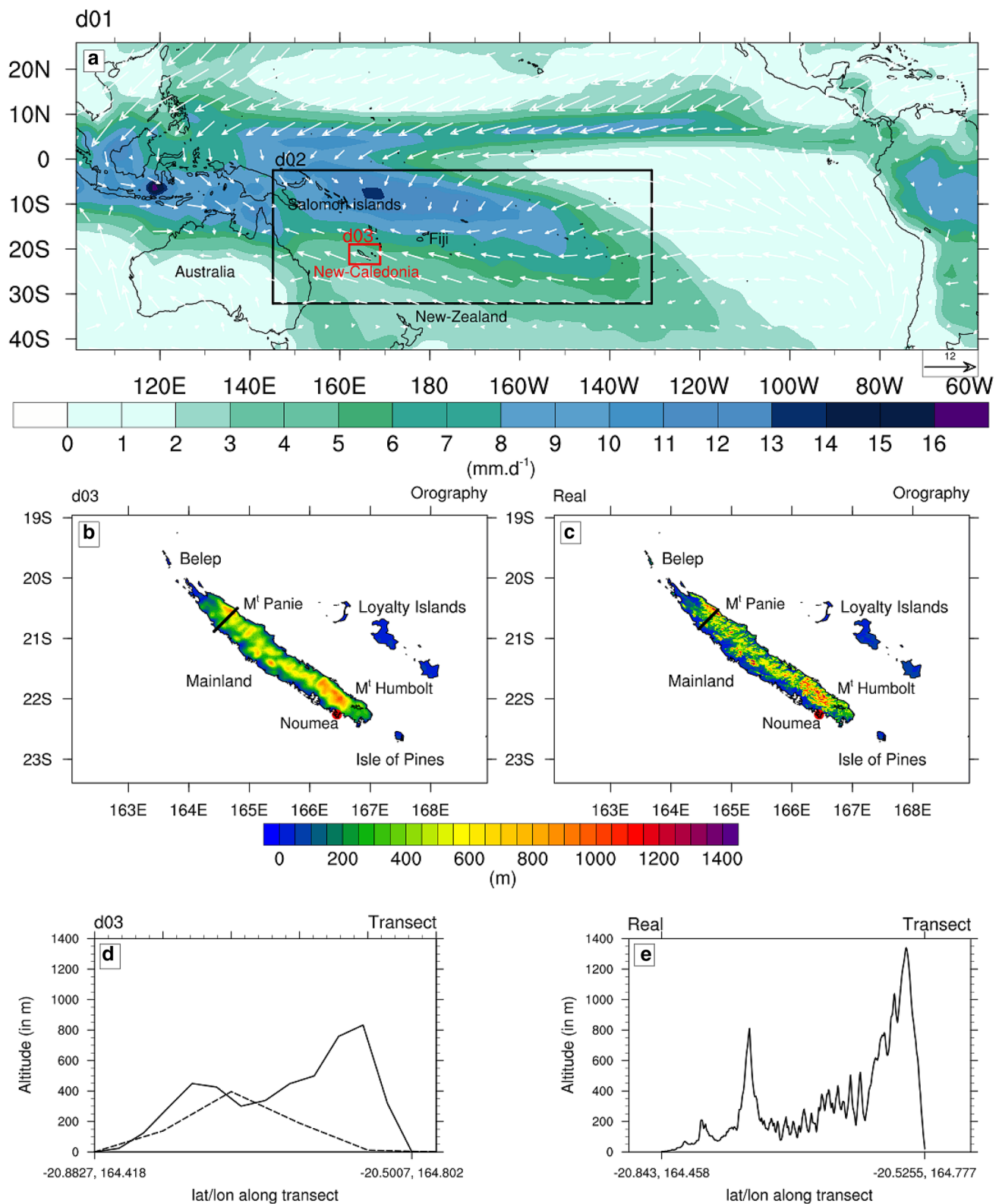
Fig. 1 **a** Model domains with DJF climatology for precipitation (shading; in mm.day^{-1}), and near surface winds (vectors; in m.s^{-1}) from observations (CMAP) and ERA5 reanalysis, respectively. The spatial extent of 20 km and 4 km-resolution domains are represented by the black box and the red box, respectively. Orography (in m) of (**b**) of the innermost 4 km-resolution domain, and (**c**) real orography of the NC at 80 m resolution. Elevation transect (in m) through Mt Panié from the (**d**) 4-km (solid line) and 20-km (dashed line) resolution simulations, and (**e**) the real orography at 80 m resolution. The black lines in (**b**) and (**c**) panels show the transect lines

by the largest lagoon in the world, which has been classified as a world heritage natural site by the United Nations Educational, Scientific and Cultural Organization (UNESCO). With 49 plants and 1.6 endemic vertebrate species per 100 km^2 (Chazeau 1993; Myers 1988; Myers et al. 2000), NC is ranked among the 25 top world biodiversity hotspots over land (Myers et al. 2000; Payri et al. 2019). This precious environment is however vulnerable to abrupt climatic changes and especially to drought stress (Brodribb and Field 2000; Ibanez et al. 2017; Pouteau et al. 2015). Assessing the impact of anthropogenic forcing on NC rainfall is hence necessary, from both a socio-economic and conservation viewpoint.

Located at about 21°S, NC hosts both temperate and tropical climate features. Its seasonal cycle is strongly influenced by the seasonal migration of South Pacific Convergence Zone (SPCZ), a diagonally-oriented convective area (Fig. 1a). The SPCZ extends southeastward during austral summer, becoming a major rainfall source for many South Pacific Islands, but is confined to the Salomon Sea during austral winter. This yields warm and rainy conditions during austral summer over NC, while austral winter is colder and drier (Ceccarelli et al. 2013; Payri et al. 2019). Superimposed to that seasonal cycle, large-scale climate fluctuations modulate the NC climate (Lefèvre et al. 2010). This includes the Madden–Julian Oscillation (Madden and Julian 1994) at intraseasonal timescales, the El Niño/Southern Oscillation (Timmermann et al. 2018) at interannual timescales and the Interdecadal Pacific Oscillation (Power et al. 1999) at decadal timescales. At higher frequency, synoptic conditions around NC, the so-called weather regimes, are controlled by the SPCZ location and intensity, the subtropical jet stream and by mid-latitude low-pressure systems (Lefèvre et al. 2010). Other high frequency phenomena such as tropical cyclones and polar depressions (Payri et al. 2019) also occasionally impact NC. Our knowledge of past and future New Caledonian precipitation trends associated with climate change is so far scarce. Over the historical period (1951–2015), a non-significant negative trend (between 0 and − 30 mm/decade) is observed in NC precipitation change (McGree et al. 2014, 2019). The future climate response to anthropogenic forcing is generally derived from the analysis of global ocean–atmosphere general circulation models gathered in the Coupled Model Intercomparison Project (CMIP) database (Taylor et al. 2012). CMIP5 models project a non-significant increase in precipitation (+ 3%) by the end of twenty-first century over the entire southwestern Pacific scale (Brown et al. 2013; Dutheil et al. 2019).

CMIP models have an horizontal resolution of the order of 100–200 km. This does not allow representing the marked orography of the NC mainland, which plays an essential role in its rainfall distribution. The NC main orographic feature is a mountain range oriented along the main axis of NC with a mean altitude of about 800 m (Bonvallot et al. 2012) that hugs the east coast (Fig. 1b–e). The highest peaks (Mont Panié and Mont Humboldt, to the north-east and south-east) are about 1600 m high. They form the two main obstacles to the trade-wind flow and peak below the trade-wind inversion located at about 2.5–3 km height (Lefèvre et al. 2010). The Mainland mountain range is irregular, interspersed with east–west valleys that form wide gaps. In comparison, the Loyalty Islands, Isle of Pines, and Belep are low-lying islands with heights below 150 m (Fig. 1b, c). An accurate representation of the NC orography is thus a prerequisite to realistically simulate the NC rainfall. Not only do CMIP models have insufficient spatial resolution to resolve NC features, but they also display large systematic biases in the western Pacific, such as an equatorial cold bias (the "cold tongue " bias, e.g. Li and Xie 2014) and a too zonal SPCZ that extends too far eastward (often referred to as the "double ITCZ" bias, e.g. Grose et al. 2014). These biases strongly limit our confidence in the CMIP models projections for this region (Brown et al. 2015). In order to provide more reliable projections of future NC climate changes, Cavarero et al. (2012) used a statistical method based on a few meteorological stations to downscale the projected temperature and precipitation changes from CMIP3 model projections over NC at these stations. While such a technique partly addresses the resolution issue by doing an orography-dependent downscaling at given points, it does not resolve the issues associated with CMIP model biases nor does it give the spatial structures at scales relevant for the entire territory.

Dynamical downscaling is another way of bridging the gap between CMIP models and fine-scale projections. This technique consists in performing experiments at higher horizontal resolution than CMIP models using regional or global atmospheric models forced by CMIP projections at their boundaries, which allows representing more accurately the topography of NC Mainland. For instance, Fig. 1d shows that a 4 km representation of the real topography (Fig. 1f) is correct while its representation at scales used in the highest-resolution climate models cannot reasonably account for the mountain chain (dashed line on Fig. 1d). The above-mentioned CMIP models biases however propagate into the regional model if directly applied at its boundaries (e.g. McClean et al. 2011; Small et al. 2014). A commonly used strategy to alleviate this shortcoming is to prescribe "climate change anomalies", i.e. prescribe observed present-day surface and lateral boundary conditions, onto which the anomalous ensemble-mean CMIP projected changes are added (e.g. Dutheil et al. 2019; Knutson et al. 2008). This approach is sometimes referred to as pseudo-global warming (PGW) downscaling. This PGW method hence allows removing the biases induced by systematic present-day boundary conditions errors in CMIP models. These present-day biases however also influence the regional climate response to

anthropogenic forcing (e.g. Held and Soden 2006; Xie et al. 2015). Li et al. (2015, 2016) for instance demonstrated that the dry bias over the western equatorial Pacific results in a strong projected western equatorial Pacific surface warming response, probably due to an underestimation of the convective feedback. The SST warming spatial pattern can be corrected on the basis of the statistical relation between the present-day biases and projected changes, a method commonly referred to as "observational constraint" or "emergent constraint" (e.g. Bracegirdle and Stephenson 2013). Li et al. (2016) applied this methodology to reduce biases in the SST change projected by CMIP models in the tropical Pacific, resulting in a reduction of the ensemble-mean western Pacific warming and of the spread in projected SST changes across models. Dutheil et al. (2019, 2020) have recently applied this emergent constraint method within the PGW framework to force a regional atmospheric model over the western Pacific. Their results demonstrate that simulations forced with bias-corrected CMIP SST projections yield a considerably larger (~25%) rainfall reduction under the SPCZ than in those forced with uncorrected SST CMIP projections (~7% rainfall reduction).

While Dutheil et al. (2019) provided more reliable rainfall projections at the regional scale, these projections remain way too coarse (~100 km) for resolving individuals islands orographic features. The present study aims at providing more reliable rainfall projections for the NC archipelago by further downscaling the climates from CMIP model, and is to our knowledge the first effort to dynamically downscale climate change over NC. To that end, we use a South Pacific regional configuration of the Weather Research and Forecasting (WRF) model similar to that in Dutheil et al. (2019) by using a PGW downscaling method where the projected SST anomalies are corrected following Li et al. (2016)'s methodology. As in Dutheil et al. (2019, 2020), we also employ a nesting strategy to increase the horizontal resolution up to ~4 km around the NC archipelago in order to improve the NC topography and the reliability of climatic projections at the island scale. A similar strategy had been applied by Zhang et al. (2016ab) to downscale the Hawaiian climate, although that study did not attempt correcting the projected SST change as we do in the present work. The framework employed here allows investigating the future response of the NC climate to anthropogenic forcing using an approach that alleviates biases induced by the historical and projected SST errors in CMIP models. The paper is organized as follows. Section 2 describes the experimental design. Section 3 provides a thorough evaluation of the NC rainfall characteristics simulated by our present-day simulation. Section 4 discusses the future changes in the NC rainfall climatology and assesses the projected changes in the NC weather regimes and links them to precipitation changes. Section 5 provides a summary and a discussion of our results

against those of previous studies and gives some perspectives for future works.

2 Material and methods

2.1 Observations datasets

Daily precipitation amounts were provided by Meteo-France and the hydrological services of New Caledonia. The high-resolution dataset encompasses 92 time series over the 15-year period 2000–2014. Rainfall data have already been checked for gross errors (instrumental failures, time coding, digitization, etc.) and spatial inconsistencies (isolated wet/dry report, outliers) by their respective provider. Their observing and climatological pratices comply with WMO standards. Rain gauges are disseminated all over the territory (not shown). Daily precipitation amounts are averaged into monthly means, which are then spatially averaged using an interpolation scheme that accounts for the locations of the stations, including their altitude to account for orographic effects (i.e. AURELHY Krigging method developed at Meteo-France; Benichou and Le Breton 1987). We also used Climate prediction center Merged Analysis of Precipitation (CMAP, Xie and Arkin 1997) for climatological precipitation on Fig. 1, and European Centre of Medium Range Weather Forecasting Re-analysis 5 (ERA5) (https://confluence.ecmwf.int/display/CKB/ERA5+data+documentation) to validate the present-day weather regimes.

2.2 WRF regional model configuration

We use the Weather Research and Forecasting Model version 3.9.1 with a parent domain at 105-km resolution that encompasses the tropical Pacific region [101°E–59°W; 26°N–42°S] (Fig. 1a). To simulate the NC climate, we further include a 21-km resolution two-way nested domain located over the Southwest Pacific [145°E–130°W; 32°S–2°S] as in Dutheil et al. (2020). A third level of nesting, a 1-way nesting, allows to reach a 4.2 km horizontal resolution over the NC archipelago [162°E–169°E; 23.5°S–19°S] (Fig. 1a). The three domains share the same 32 vertical terrain-following sigma levels (17 levels below 700 hPa). The main configuration discussed here uses the Lin et al. (1983) microphysics scheme, the Community Atmosphere Model (Collins et al. 2004) shortwave and longwave radiation scheme, the University of Washington planetary boundary layer (Bretherton and Park 2009) with the Monin–Obukhov surface layer parameterization, and the Noah land surface model (Chen and Dudhia 2001). The physical configuration is similar that used in Dutheil et al. (2019), except that the Zhang and McFarlane (1995) parameterization scheme for subgrid-scale convection is disabled in 4.2 km-resolution domain,

considering the convection is explicitly resolved at this resolution.

A present-day simulation is first performed over the 2000–2016 period (17 years). Surface and lateral boundary conditions for the parent domain (105 km) are taken from 6-hourly outputs of the NCEP2 reanalysis (Kanamitsu et al. 2002). A future simulation (labelled CC) is conducted by adding the projected changes in surface (SST) and lateral (wind velocity, temperature, humidity) boundary conditions derived from the CMIP5 projections under the RCP8.5 scenario. The projected changes are computed as the ensemble-mean difference between late twenty-first-century (2080–2099) minus historical simulations (1989–2009) across 31 CMIP5 models. This methodology allows correcting for present-day SST biases but assumes no change at non-seasonal timescales at the boundaries between the present and future climate.

Projected CMIP5 SST changes are also corrected using the "emergent constraint" method of Li et al. (2016), relying on the statistical relationship between the present-day precipitation bias over the western equatorial Pacific (black box [140°E–170°W; 2°S–2°N] on Fig. 2a) and the projected SST change across 31 CMIP5 models (Fig. 2b). The significant correlation (− 0.56, p-value < 0.001; see Fig. 2b) indicates that the drier the present-day west Pacific, the stronger the projected SST warming in the equatorial western Pacific. This linear relationship is used to correct the projected SST warming pattern of each model. This correction reduces the ensemble-mean warming in the South and equatorial western Pacific (Fig. 2d vs. 2c). Dutheil et al. (2019) showed that the corrected SSTs yield a considerably larger SPCZ drying (~ 30%) than in the uncorrected simulations (~ 7% decrease) in the future, as a response of the SP circulation and humidity convergence to altered SST gradients.

Finally the CO_2 forcing is kept constant in the present-day simulation at a level representative of the recent period (379 ppm), while in both climate change simulations we apply a constant CO_2 forcing representative of the RCP8.5 projections at the end of the twenty-first century (845 ppm).
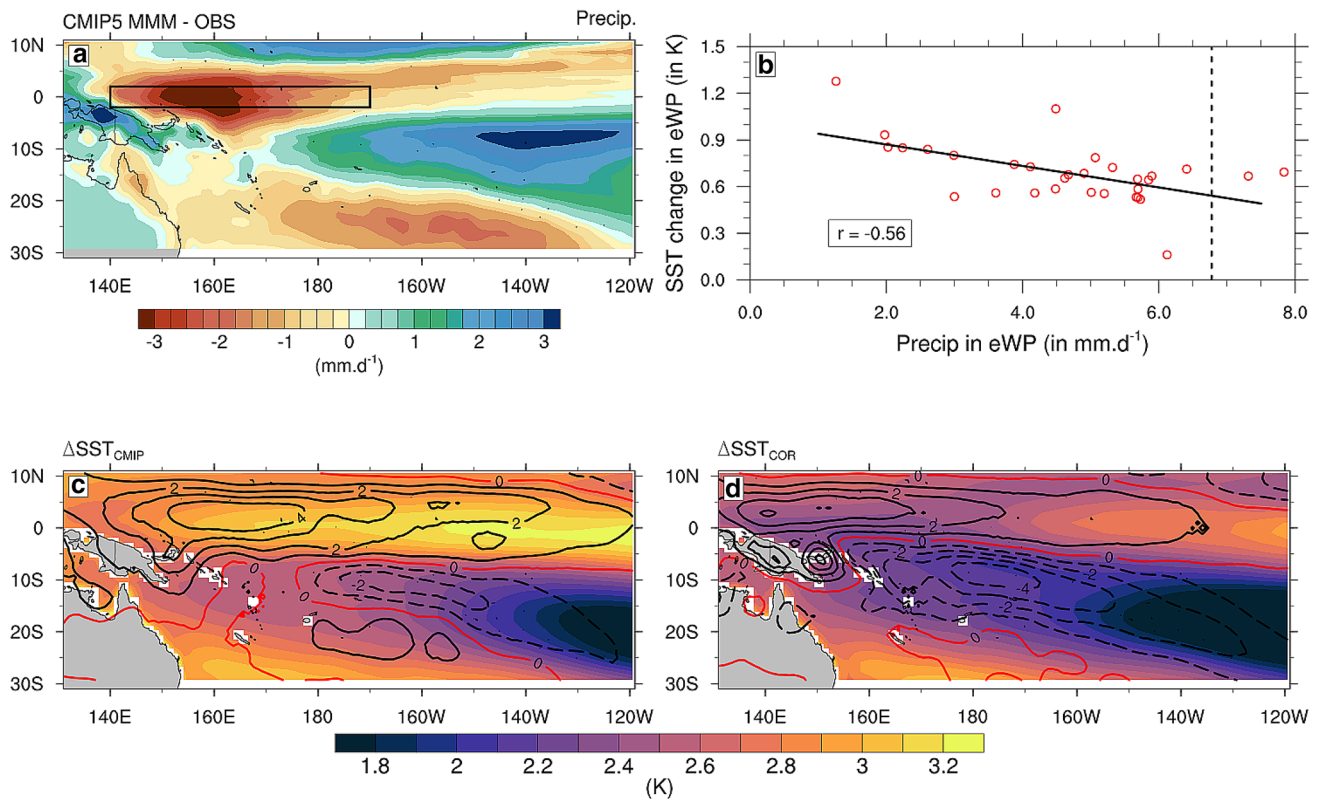

Fig. 2 Top: (**a**) Multi-model mean CMIP5 of precipitation bias (in mm.day^{-1}) relative to observations (CMAP). **b** Relationships between the SST projected changes (°C) and the historical mean precipitation (mm.day^{-1}) in the equatorial western Pacific (160°E–170°W;2°S–2°N) among 31 CMIP5 models (red dots). The inter-model correlation (r) is shown at the bottom-left. The dashed lines on the panel b denote the observed mean precipitation in the equatorial western Pacific. Bottom: DJF climatology (shading, in °C) of (**c**) ΔSST_{CMIP} and (**d**) ΔSST_{COR}. The contours represent the DJF climatology of precipitation changes (in mm.d^{-1}) assiocated to SST warming pattern. The dashed lines indicate negative values, while the thick lines indicate positive values

2.3 Weather regimes

The weather regime classification is a statistical method that allows determining the main modes of synoptic atmospheric variability over a region, i.e. recurrent meteorological conditions (e.g. Lefèvre et al. 2010). This analysis is particularly relevant to understanding the reasons for precipitation changes in NC because the spatial distribution of precipitation is controlled by both orography and flow orientation from synoptic atmospheric structures. The synoptic atmospheric structures control the amount of moisture transported in the vicinity of New Caledonia, while the orography has an enhanced effect on convection by air uplifting when the wind flow is perpendicular to the relief. As most of the changes simulated for the future are observed during the warm (austral summer) season in NC, we will focus on summer weather regimes in the following.

We determined these weather regimes based on the simulated surface winds for 16 warm seasons (2991 days) in the "d03" domain (red box in Fig. 1a). The data was centered and reduced at every grid point. A principal component analysis (Jolliffe 2011) was then performed on the 2991 days of u and v data to reduce the spatial dimensions and filter the smallest scales of spatial variability. The data was filtered by only keeping signals that project on the first 9 principal components, which represent 95% of the total variance (not shown). The 2991 daily fields were then classified with a k-means classification algorithm (Diday 1971). Determining the optimal number of cluster is a classic issue of the k-means classification algorithm: many methods have been developed to choose the number of clusters. The 'NbClust' function in the factoextra R package allows comparing the results from 26 different methods (Charrad et al. 2014). The 4 clusters presented here correspond to a consensus between these 26 methods (16 methods suggest 3 or 4 clusters, with 4 being the most common result, not shown), in agreement with the studies of Lefèvre et al. (2010), Leroy (2006) and Specq et al. (2019). We then produced precipitation composites for each regime.

2.4 Extreme precipitation

Precipitation extremes can cause severe damages on the NC population (e.g. flash floods) and environment (e.g. strong sediment release into the lagoon) (Baltzer and Trescases 1971). Such extremes have multiple causes (e.g. tropical cyclones, spells from the Tasman Sea fronts) and their contribution to the annual mean rainfall is important (Maitrepierre and Caudmont 2007). To assess their characteristics and how they may evolve in the future, we calculated four extreme rainfall indices derived from the ClimPact2 package developed by the World Meteorological Organization (WMO) Expert Team on Sector-specific Climate Indices (ET-SCI) (https://github.com/ARCCSS-extremes/climpact2):

- R30mm = Annual number of days when PR ≥ 30 mm.
- R99P = Annual sum of daily PR > 99th percentile.
- R99PTOT = 100*R99P /PrTOT
- SDII = Annual PR divided by the number of wet days (when PR > = 1.0 mm)

where PR represents the daily precipitation; PrTOT the annual sum of all PR values above 1 mm.day^{-1}. We chose to analyze these four indices because they characterize different aspects of precipitation extremes: the frequency of strong rain events (R30mm) in days, their total annual precipitation (R99P) in mm, their contribution the annual mean (R99PTOT) in %, and the typical wet day precipitation intensity (SDII) in mm d^{-1}. As discussed in the introduction, water resource management in NC is regularly facing water shortages issues. Changes either in the frequency or the intensity, and the contribution of extreme rainfall to total annual rainfall have important impacts.

2.5 Divergence of moisture flux

To understand the precipitation changes we used the vertically integrated moisture flux divergence change, which is in general dominated by the contribution of the boundary layer in the tropic regions (Kuo 1965, 1974). The vertically integrated boundary layer moisture flux divergence change from PD to CC can be decomposed into its "thermodynamical" and "dynamical" components, which respectively represent the influence of moisture and circulation changes (e.g. Zhang et al. 2016b):

– Thermodynamical effect:

$$\delta TH = \int_{Psfc}^{Ppbl} \nabla \cdot \left(\overline{u} q' \right) dp \qquad (1)$$

– Dynamical effect:

$$\delta DYN = \int_{Psfc}^{Ppbl} \nabla \cdot \left(u' \overline{q} \right) dp \qquad (2)$$

where u is the horizontal wind vector, q is the specific humidity, the overbar represents the present day values and primes represent the futures changes. Psfc represents the surface pressure, and Ppbl is defined here as Psfc minus 400 hPa. The u'q' cross term is not discussed here as δTH and δDYN dominate the balance in the region of interest (not shown).

3 Evaluation of the present-day simulation

3.1 Rainfall climatology

The observed averaged rainfall NC archipelago is about 5.1 mm.d^{-1}. Its distribution is however spatially contrasted over the NC mainland (Fig. 3a), with a far wetter east coast (~ 7 mm.d^{-1}) than the west coast (~ 3 mm.d^{-1}). The wettest spots (~ 12 mm.d^{-1}) are located close to the two main peaks, Mt Panié and Mt Humbolt (Fig. 1bc). The driest regions (~ 2 mm.d^{-1}) are the valleys at the foot of these mountains. The PD simulation reproduces the contrasted rainfall distribution between the east and west coasts and the high rainfall over orography (rainfall exceeds 12 mm.d^{-1} over the two main peaks, Fig. 3b vs. 3a). There is however an overall rainfall overestimation in the PD simulation compared to both

AURELHY and the rain gauge stations (not shown). The NC average rainfall is 6 mm.d^{-1} in the PD simulation, i.e. an overestimation of about 18% compared to observations (5.1 mm.d^{-1}). In contrast, CMIP5 models poorly simulate the mean rainfall over NC, with a ~ 45% underestimation and do not simulate the contrasted rainfall distribution between the east and west coasts (Fig. 3c).

As mentioned in the introduction, the seasonal SPCZ displacement brings highest rainfall during boreal summer over the NC archipelago (Fig. 4). Highest seasonal precipitation rates (~ 10 mm.day^{-1}) occur in March while lowest rates (~ 2 mm.d^{-1}) occur in late austral winter (yellow curve on Fig. 4). The PD simulation captures this seasonal contrast (blue curve on Fig. 4), despite a ~ 0.6 mm.d^{-1} overestimation of precipitation rates during austral summer and ~ 1.4 mm. d^{-1} overestimation during winter.
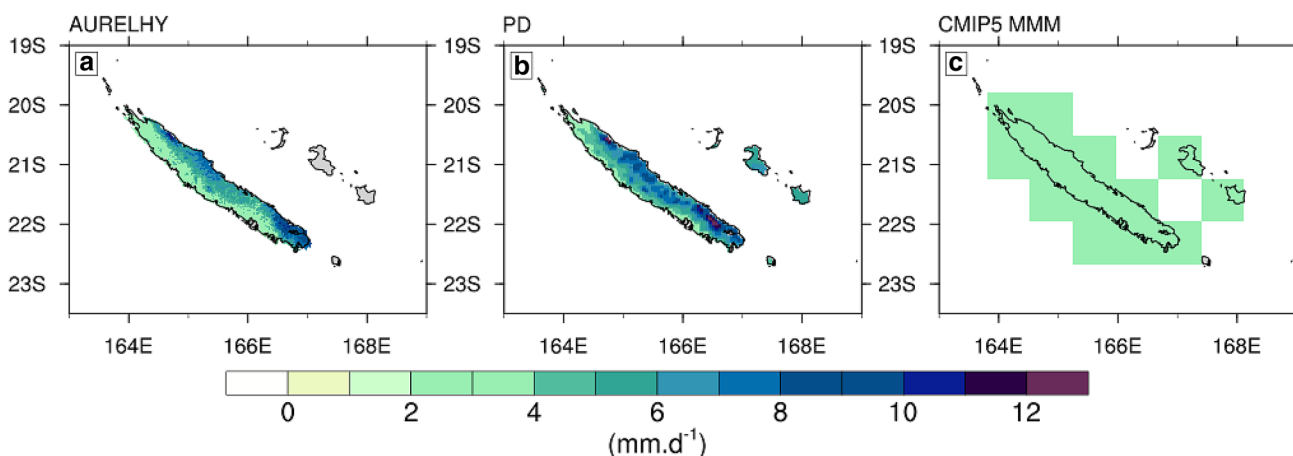

Fig. 3 Annual mean of precipitation (in mm.day^{-1}) over the 2000–2014 period from (**a**) observations interpoled with AURELHY method, (**b**) the PD simulation, and (**c**) CMIP5 MMM interpoled over 1° resolution grid

Fig. 4 Seasonal cycle of precipitation (in mm.day^{-1}) averaged over the Mainland and the 2000–2014 period from observations interpoled with AURELHY method (yellow curve) and the PD simulation (blue curve)
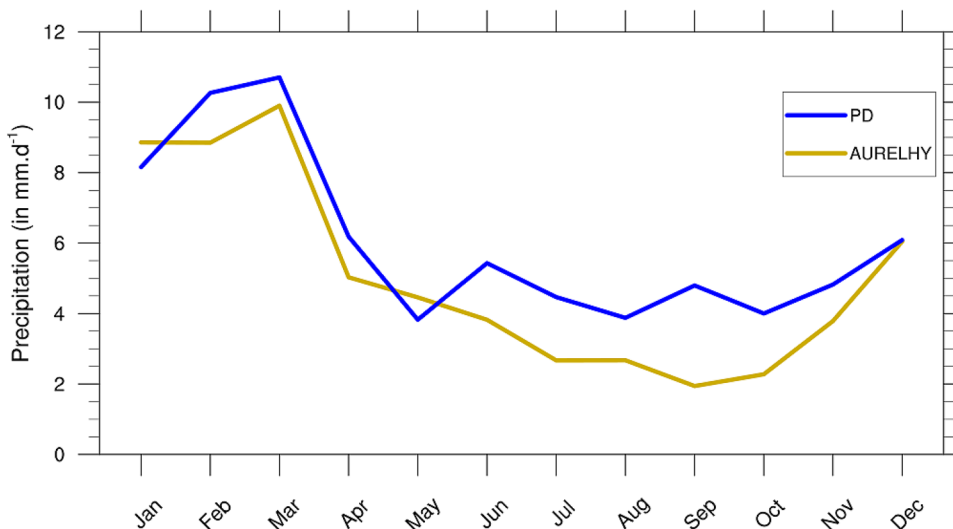
Extreme precipitations in both observations and PD simulation are computed using ClimPact2 package for a set of selected rain gauges stations. The package used to calculate extreme indices indeed requires daily time series, which are not available for all rain gauges stations. We therefore selected 8 stations where daily data were available and that sample the entire NC archipelago (Fig. 5a): 2 stations overs Loyalty islands (Lifou and Maré), 3 stations over west coast (Paita, Nouméa, and Koumac), 2 stations over east coast (Ponérihouen and Houailou), and 1 station in the mountain range (La Foa). There are on average ~ 15 days when daily precipitation exceeds 30 mm (R30mm) across the selected stations (Fig. 5b). R30mm maxima are located on the east coast (e.g. 24 days at Ponerihouen) and minima on the west coast (e.g. 8 days at Nouméa). Loyalty islands have intermediate (between east and west coast) values of R30mm. The rainy day precipitation intensity SDII (Fig. 5c) is on average ~ 13 mm.d^{-1}, with maxima on the east coast (e.g. 17.5 mm.d^{-1} at Ponerihouen) and minima on the west coast (e.g. 9.5 mm.d^{-1} at Nouméa). Finally, extreme precipitations on average represent ~ 10% of the total precipitation (R99PTOT; Fig. 5d), and the total annual precipitation from very heavy rain days (R99P; Fig. 5e) is ~ 274 mm. This last index exhibits maximum values on the east coast (e.g. 330 mm at Ponerihouen) and minimum values on the west coast (e.g. 133 mm at Nouméa). These four indices are reasonably well captured by PD simulations (Fig. 5), despite an obvious overestimation of the simulated SDII (Fig. 5c) and R30mm (Fig. 5b) indices at most locations.

Overall, this section demonstrates that despite a ~ 18% rainfall overestimation the PD simulation is able to capture reasonably well orography-induced spatial patterns in precipitation, the rainfall seasonal cycle over NC, and present-day extreme rainfall statistics. Our model configuration is thus an appropriate tool to examine the future changes in rainfall over NC.

3.2 Weather regime

Synoptic conditions responsible for the precipitation changes are identified through a classification of atmospheric conditions into weather regimes as described in the methods section. This section describes (Fig. 6) and validates (Fig. 7) the simulated present-day regimes structures and statistics, while regimes changes in response to climate change are further discussed in Sect. 4. In this section we restricted our analysis to the warm season, which accounts for ~ 80% of the precipitation future decrease as discussed in Sect. 4.

The first weather regime is associated with a low-pressure system located about 500 km south of NC (Fig. 6a, b). The resulting northwesterly flow over NC transports moist air from the western part of the SPCZ towards NC (Fig. 6a), yielding high precipitation rates over the archipelago,

especially over the southeastern mainland when the wind flow turns from north-west to north resulting to an orographic enhancement (Fig. 6b) of precipitation. While this regime drives the largest rainfall rates over NC (12.6 mm. day^{-1}), it only contributes to 18% of the total summer rainfall because it is relatively infrequent (~ 11%). The second regime is associated with a low-pressure located to the northeast of NC. The resulting south-southeasterly flow over NC advects cold and dry air from the Tasman Sea toward NC (Fig. 6c, d). This regime is associated with the driest conditions over NC (4.3 mm.day^{-1}) and hence contributes only modestly to the total summer rainfall amount (10%). The third regime (Fig. 6e, f) is a southeasterly flow and is commonly referred to as the trade wind regime (see Lefèvre et al. 2010). It is the most frequent weather regime during the hot season (~ 38%), associated with an intense high-pressure system in the northern Tasman Sea and a low-pressure system north of NC. The resulting strong southeasterly winds push moist air from the eastern part of the SPCZ towards NC (Fig. 6e), inducing rainfall over the eastern coast of the mainland (Fig. 6f). Because of its frequent occurrence, it is the second contributor to the total summer rainfall (34%) in the current climate. The fourth regime corresponds to a more easterly-oriented flow (Fig. 6g, h), associated with a high-pressure zone southeast of our simulation domain, towards the Kermadec Islands (Fig. 6g). The orientation of this flow contributes to the production of large amounts of precipitation on the east coast of NC induced by orographic lifting (Fig. 6h), contributing to a large part of the total summer rainfall amount (38%).

Figure 7 compares these weather regimes from the PD simulations to those calculated from ERA5 reanalysis. Weather regimes from these two datasets are generally in good agreement (Fig. 7a–d vs. 7e–g), with reasonably similar wind structure and magnitude as well as number of occurrences. Nevertheless wind speed are overestimated by ~ 1.5 m.s^{-1} in the PD simulation for regime 1, 2 and 3. In addition, while wind direction is northerly in ERA5 for regime 1, it is north-westerly oriented in the PD simulation.

4 Response to climate change

In this section, we investigate the mean and extreme precipitation changes in NC in response to anthropogenic forcing. First, we describe the mean precipitation changes in the CMIP5 multi-models mean (MMM), and then compare them with our simulations to assess the impact of our downscaling strategy, which involves both a much better spatial resolution and a methodology that aims at mitigating CMIP model systematic biases. We then project present-day weather regimes into future conditions to link them to precipitations changes. Finally, we investigate the extreme precipitation changes
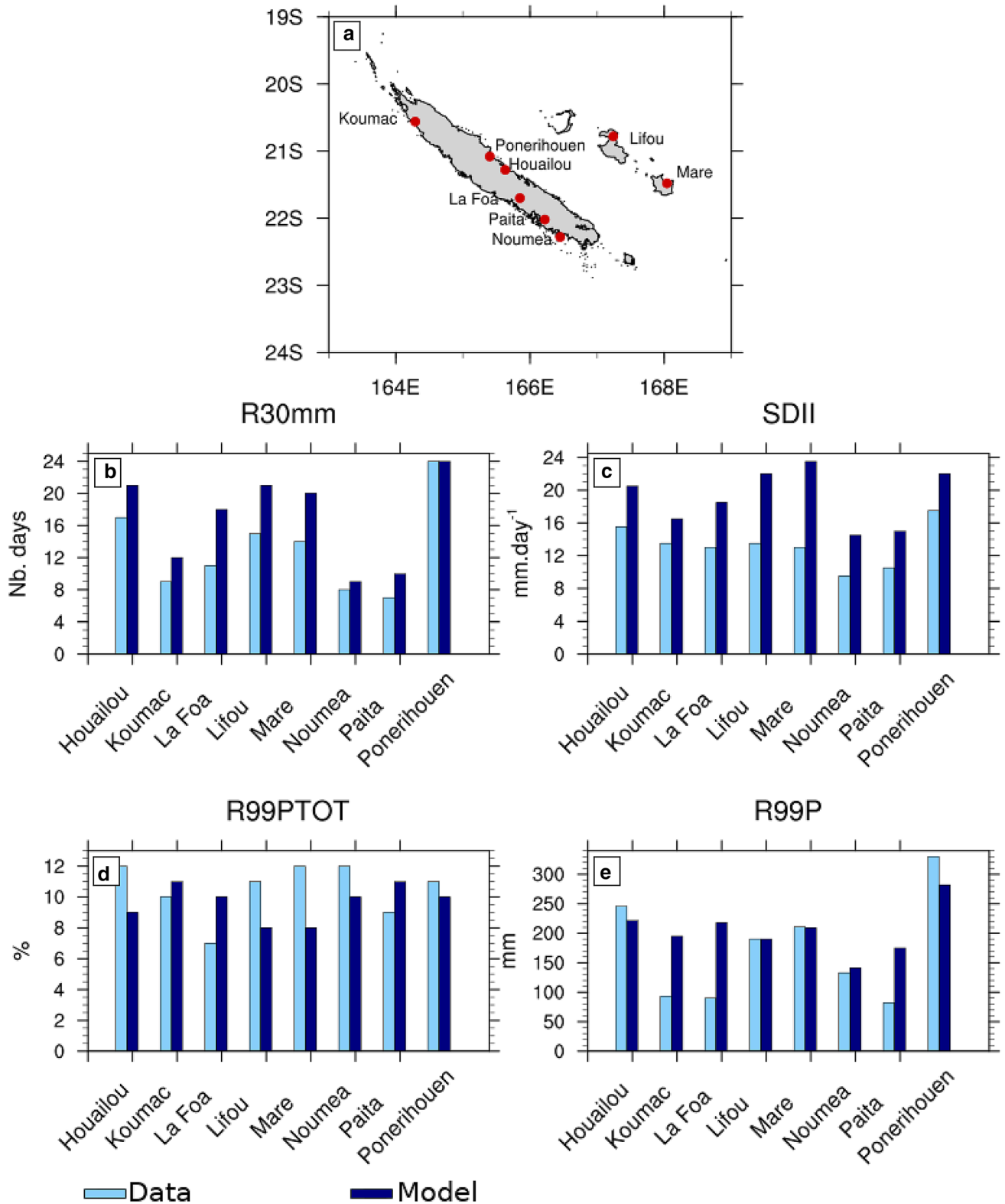
Fig. 5 **a** Map representing New-Caledonia archipelago. The eight rain gauge stations are located by red dots on NC map. Barplots representing 4 extreme rainfall indices: (**b**) R30mm, (**c**) SDII, (**d**) R99PTOT and (**e**) R99P at 8 rain gauge stations. Light blue bars represent the values mesured at rain gauge stations and dark blue bars the values simulated in PD

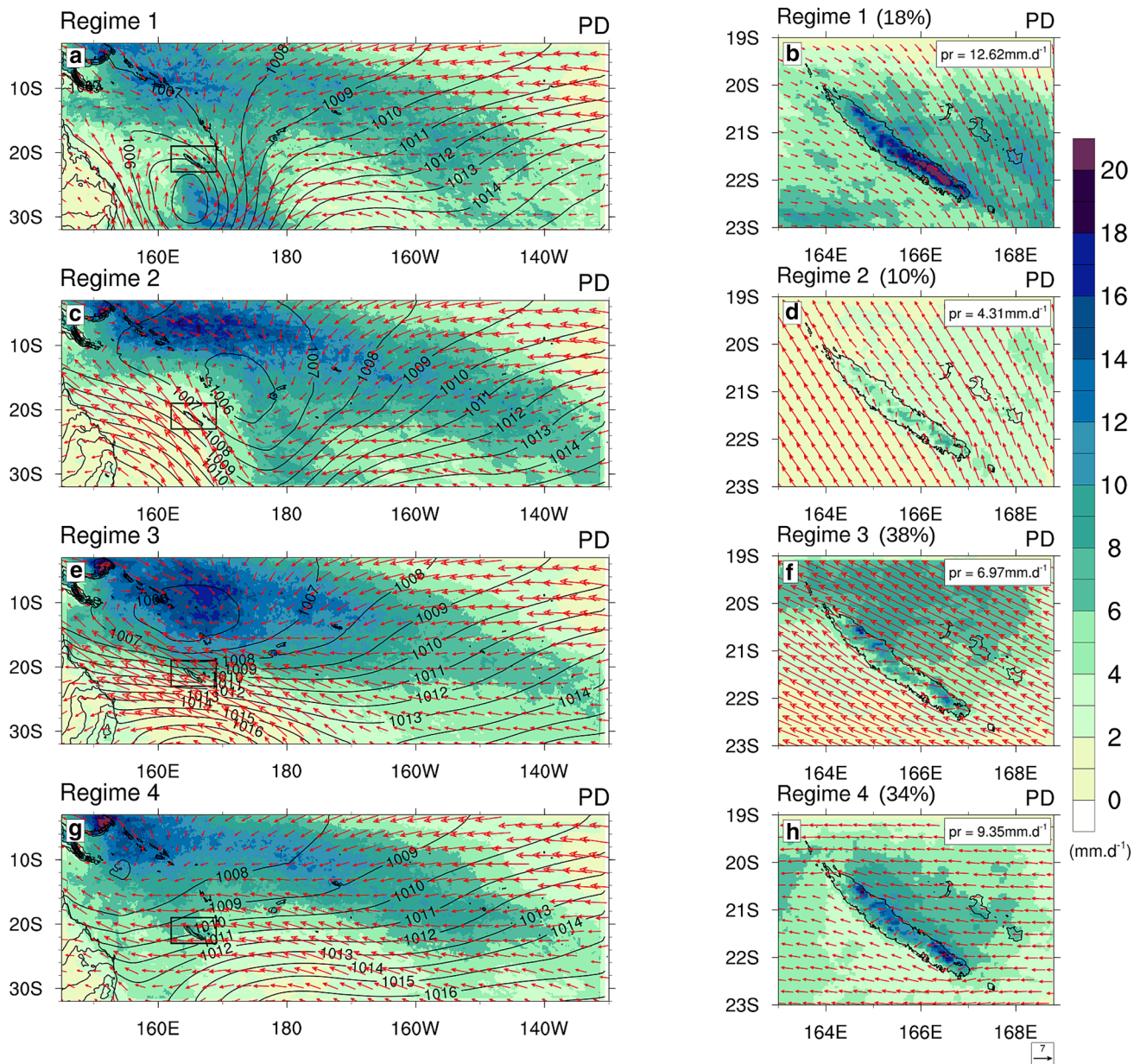**Fig. 6** Average of precipitation (shading; mm.day^{-1}), near surface wind (vectors; m.s^{-1}) and sea level pressure (contours; hPa) for regime 1 (1st row), regime 2 (2nd row), regime 3 (3rd row), regime 4 (4th row) in d02 (1st column) and d03 (2nd column) domains. The black box on the panels **a**, **c**, **e**, **g** shows the spatial extent of the d03 domain, and the top right-hand boxes on the panels **b**, **d**, **f**, **h** indicate the precipitation rate (in mm.day^{-1}) average over the lands for each regime. The precipitation percentage of total summer is indicated next to the regime number

from the four extreme indices R30mm, SDII, R99PTOT and R99P.

4.1 Climatological changes

The CMIP5 multi-model mean indicates insignificant changes in future precipitation over the NC archipelago at the 90% confidence level (Fig. 8a, e, i). CMIP5 inter-model distribution further reveals that changes in precipitation over NC range between − 10% (first quartile) and + 13% (third quartile) for half of the CMIP5 models (not shown). Our experimental setup on the other hand reveals a large and statistically significant decrease of precipitation over NC in response to climate change (Fig. 8b, f, j). The yearly average rainfall reduction over NC is 1.1 mm.d^{-1}, corresponding to relative drying of − 18%. This rainfall reduction exhibits a marked spatial structure, with a larger and significant drying for the southern and western part of Mainland and the
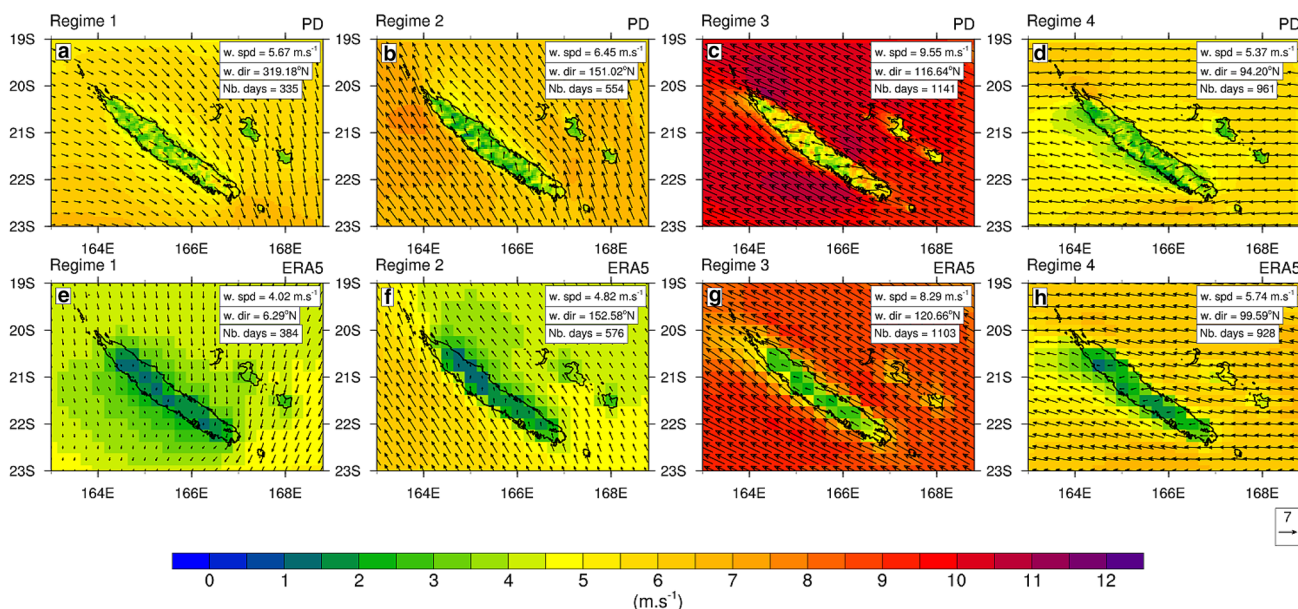
Fig. 7 Average of wind speed (shading; mm.day^{-1}), near surface wind (vectors; m.s^{-1}) for regime 1 (1st column), regime 2 (2nd column), regime 3 (3rd column), regime 4 (4th column) from PD (1st row) and ERA5 reanalysis (2nd row). The area-average wind speed, direction, and the duration of each weather regime are indicated in the top right-hand boxes

Loyalty Islands (− 20 to − 30%, Fig. 8b,f,j). The largest precipitation drop of ~ − 30% occurs in the vicinity of the capital city Nouméa (Fig. 8f). In contrast, the relative drying along the eastern coast is weaker (~ 10%) and not significant.

This projected rainfall decrease is strongly seasonally modulated. It is largest and most statistically significant during the hot season (Fig. 8c, g, k vs. 8d, h, l), which accounts for ~ 80% of the annual-mean decrease. During that season, the large and significant drying along the west coast reaches − 30% in many places, and up to − 45% in Nouméa (Fig. 8c, g, k). The mild rainfall increase over northern Mainland and moderate drying over the southern NC and Loyalty islands during the cold season are not statistically significant.

4.2 Weather regimes

The rainfall activity over NC results from the characteristics of regional weather patterns affecting the island and interaction with NC orography. Identifying projected changes of the main weather regimes in this region may provide some insights on the mechanisms driving the projected summer drying described Fig. 8. In this section, we show that precipitation increase occur in a only one weather regime (regime 1) and while 80% of the precipitation future drying in austral summer is due to the regime 3. We examine these specific regimes (regime 1 and 3) in more details by comparing the influence of the orography enhancement relative to the changes in atmospheric synoptic structure estimated from moisture flux divergence associated with these regimes.

To evaluate the changes in the characteristics between the future and present-day weather regimes, we recomputed a new set of weather regimes using future conditions (i.e. different from the present-day weather regimes). We chose this option rather than projecting the future conditions on the present-day weather regimes, because it does not assume stationarity. Stationarity is indeed unlikely because large-scale tropical conditions are strongly modified in response to climate change (Dutheil et al. 2019; Gastineau et al. 2008; Tokinaga et al. 2012; Vecchi et al. 2006, 2008). It is impossible to exactly track how one given weather regime evolves in a different climate as weather regime for different climates will differ from those calculated over present climate. Nevertheless, we can estimate which of the present-day regimes are the closest to a given future weather regime by calculating the distance between the centroids of each cluster and associating the clusters with the minimum distance. The closest future regimes will then be labeled (1–4) similarly to those of the present-day to which they are closest.

As shown on Fig. 9a–c, regime 1 experiences a strong decrease in wind speed as climate warms (3.9 m.s^{-1} vs. 5.7 m.s^{-1}) but a change in wind direction exceeding 90° (50.3°N vs. 313.5°N). This results in a surface wind hitting the NC east coast with a perpendicular angle in the future climate giving rise to a strong increase of precipitation likely induced by orographic lifting (12.6 vs. 17 mm.day^{-1}; Fig. 9b, c). This regime becomes also slightly more frequent (13.7% vs. 11.2%). Regime 2 also experiences a wind speed decrease (5.7 vs. 6.5 m.s^{-1}) but the wind direction remains
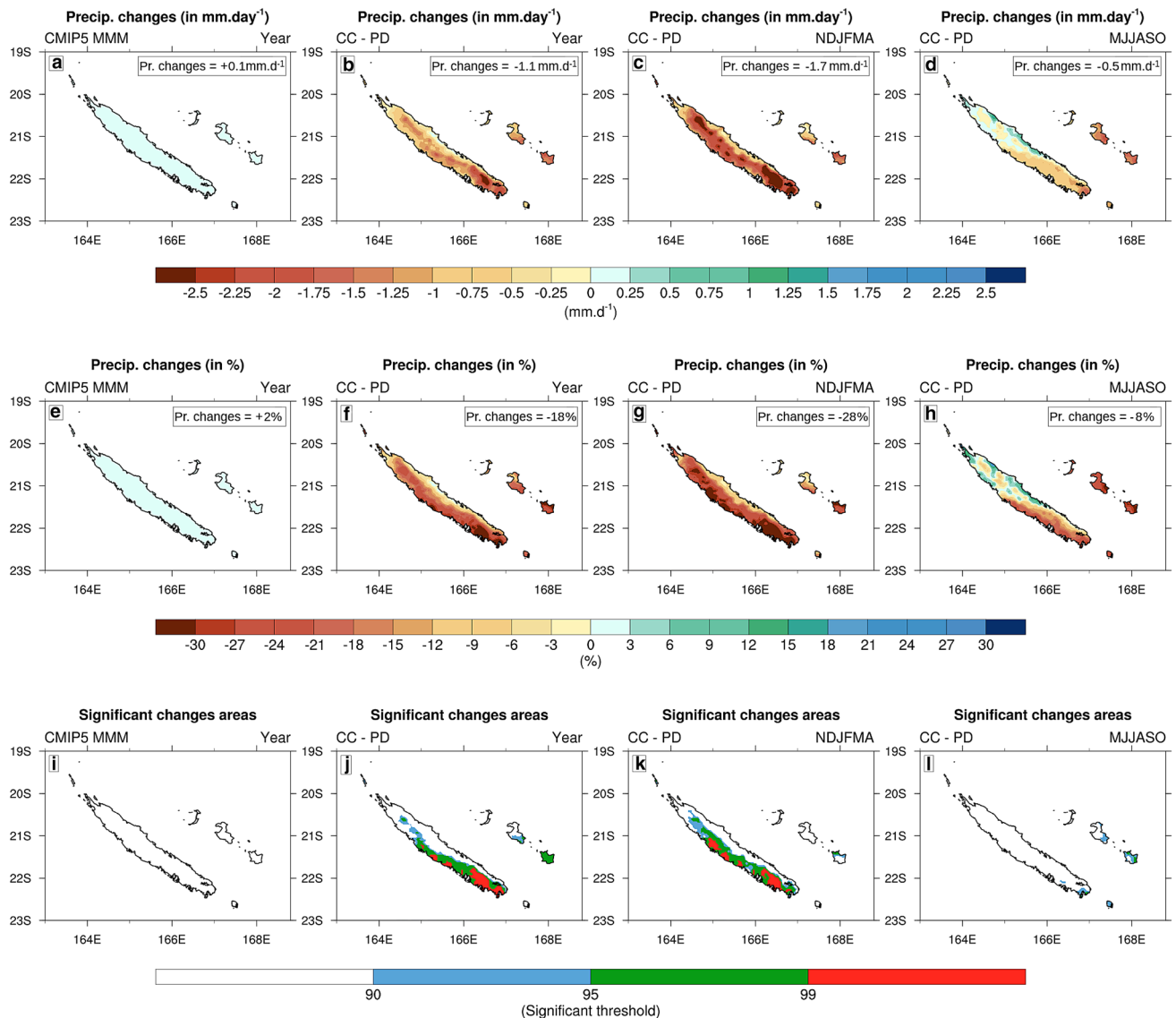
Fig. 8 Precipitation changes (1st row in mm.day⁻¹; 2nd row in %) over NC from (1st column) CMIP5 MMM, (2nd column) yearly average from the PD simulation, (3rd column) NDJFMA average, and (4th column) MJJASO average. The third row displays the region where the precipitation changes are significant according to 3 thresholds: 90% (in blue), 95% (in green) and 99% (in red) using a Mann–Whitney–Wilcoxon test. The top right-hand boxes on 1st and 2nd rows indicate the precipitation changes averaged over NC

stable (151.9°N vs. 153.2°N). Regime 2 frequency decreases (13.4% vs. 18.5%) and it is associated with drier hydrological conditions (4.3 vs. 2.8 mm.day⁻¹) (Fig. 9d–f) suggesting the influence of reduced large-scale moisture convergence to the island (see next paragraph). As for regime 2, the wind also decreases for regime 3 (9.6 vs. 8.6 m.s⁻¹). Its associated precipitation rate sharply decreases (7.0 vs. 1.8 mm.day⁻¹; Fig. 9g–i while the wind direction remains largely unchanged (116.4°N), suggesting, as for regime 2, that the projected rainfall change is not related to changes in the orography effect, but to reduced large-scale advection of moisture resulting in drier air (the dynamical effect, see next paragraph). That regime frequency decreases also

slightly (38.2% vs. 36.6%). While regime 2 was the driest regime in the present-day climate, this drying of regime 3 in the future makes it the driest regime in the future climate. Finally the wind speed increases slightly (5.8 vs. 5.4 m.s⁻¹) in regime 4 and its direction remains stable (100.6°N vs. 94.2°N). The regime frequency slightly increases (36.3% vs. 32.1%) and the precipitation rate also strongly decreases (9.3 vs. 5.7 mm.day⁻¹; Fig. 9j–l) suggesting also reduced advection of moist air to NC. In summary, all regimes except regime 1 experience a drying. The projected hot season drying is ~2.4 mm.day⁻¹ (−30.8%) of which ~2.0 mm.day⁻¹ (83%) is accounted for by the large drying due to regime 3 modification in the future.
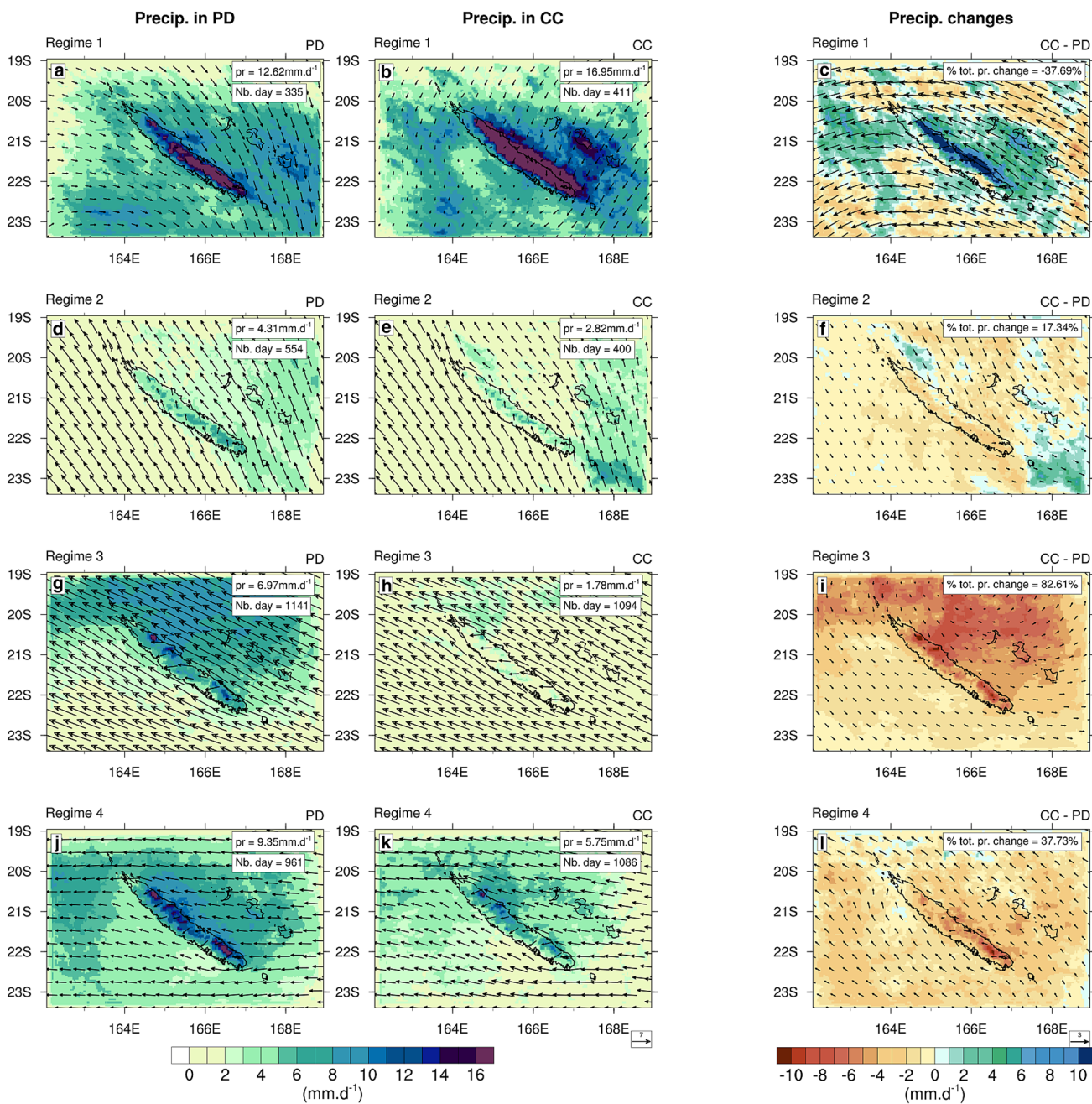
Fig. 9 Average of precipitation (shading; mm.day^{-1}), near surface wind (vectors; m.s^{-1}) for regime 1 (1st row), regime 2 (2nd row), regime 3 (3rd row), regime 4 (4th row) in d03 domain from PD (1st column), CC (2nd column) and changes (3rd column) between CC and PD

We further use the moisture convergence analysis detailed in Sect. 2 to provide insights on the mechanisms driving the simulated rainfall response to climate change (Fig. 10). For clarity, we restricted this analysis to regime 1 and regime 3, these two having the most contrasted effects on the precipitation changes (see previous paragraph). Both d02 (South Pacific) and d03 (NC) domains are examined here in order to capture changes in synoptic atmospheric structure and the orographic effect. The anomalous changes in moisture

convergence (Figs. 10d, g and 11d, g) qualitatively match those of the precipitation changes (Figs. 9c,i, 10a, and 11a), suggesting that it can provide useful hints on the mechanism responsible for the precipitation changes, as demonstrated in other studies (e.g. Widlansky et al. 2013, Zhang et al. 2016b). These analyses in regime 1 and regime 3 reveal that wind divergence changes (Figs. 10e and 11e) drive most of moisture divergence changes (Figs. 10d and 11d). In other words, the mean precipitation changes in regime 1 and 3
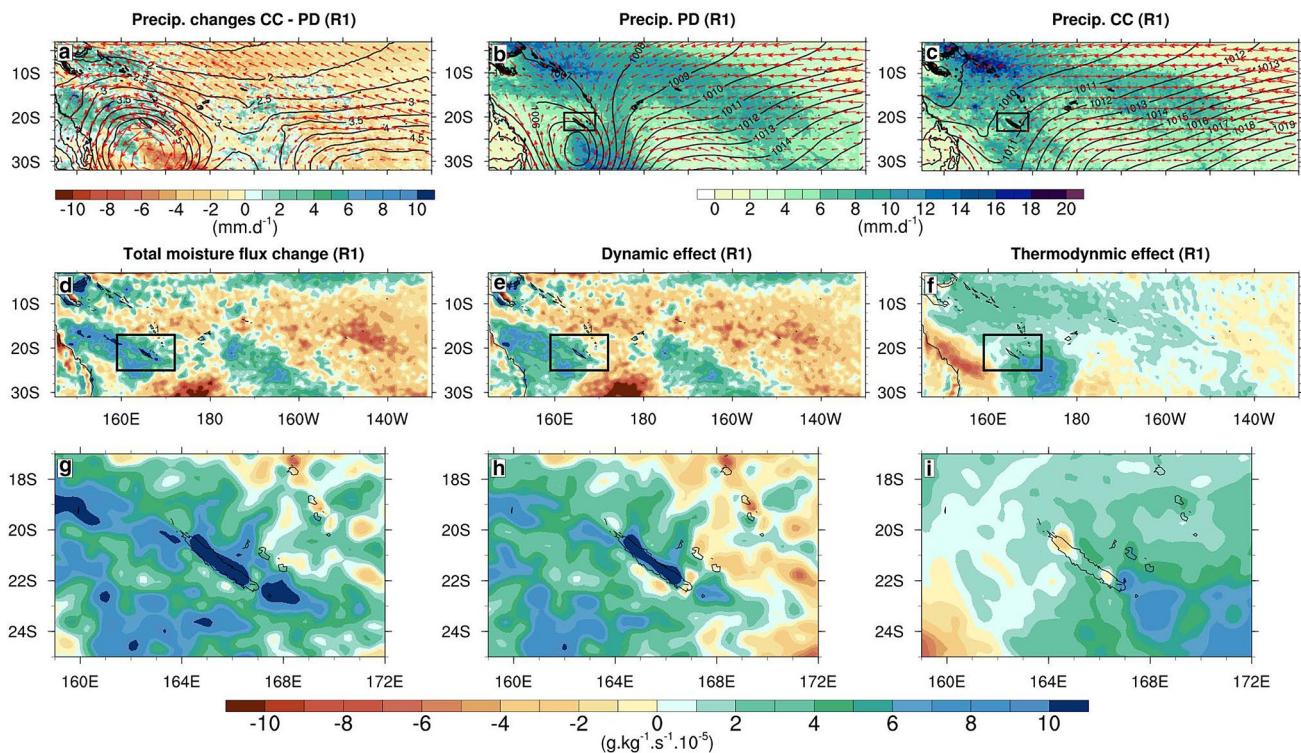
Fig. 10 Top: Average of precipitation (shading; mm.day^{-1}), near surface wind (vectors; m.s^{-1}) and sea level pressure (contours; hPa) for regime 1 (**a**) between CC and PD (**b**) in PD, and (**c**) in CC. Middle: Total (**d**), dynamic (**e**), and thermodynamic (**f**) effects on the moisture convergence (in g.kg^{-1}.s^{-1} × 10^{-5}) change (future—present) between CC and PD vertically integrated over the boundary layer for regime 1. The black boxes indicate the domain displayed on the 3rd row. Bottom: Same as the middle panels but for d03

(Figs. 10a and 11a) are mainly driven by changes in the large-scale circulation (Figs. 10e and 11e), the increase of lower-layer specific humidity due to the surface warming playing a lesser role (Figs. 10f and 11f). The remaining question is the impact of orography on these changes. In regime 1 the flow direction changes drastically and rotates from northwest (Figs. 9a and 10b) to north east (perpendicular to the relief; Figs. 9b and 10c). The slight increase in moisture convergence in the vicinity of New-Caledonia (Fig. 10d) is thus strongly enhanced by the orography (Fig. 10g) resulting to the increase of precipitation in regime 1 (Fig. 9c). However in regime 3, the flow direction remains identical between PD and CC (south-easterly and parallel to the relief; Fig. 9 g,h). In this wind flow configuration the orographic effect is very weak, and we do not observe an enhanced effect in change moisture divergence over New Caledonia. Therefore, the precipitation changes are in this case mainly explained by the changes in atmospheric synoptic structure. Figure 11a–c further displays the changes in large-scale fields associated with the changes in local weather regimes. The projected future climate reduces the intensity of low-pressure zone located north of NC associated with regime 3 while it increases the intensity of anticyclone on the Tasman Sea (Fig. 11b vs 11c). These changes result in a strong

anti-cyclonic anomaly centred on the north of NC (Fig. 11a), which is associated with a strong air subsidence anomaly (not shown) that produces a moisture flux divergence change in the boundary layer (Fig. 11d,e) and a strong decrease of precipitation in NC (Figs. 9i and 11a).

In summary, NC experiences a significant precipitation decrease (− 18%) in the future under RCP8.5 mainly located along the west coast and during the warm season (~ 80% of total annual decrease). The weather regime classification reveals that a large part (83%) of precipitation drying during the warm season is due to changes in the strong trade-wind regime (regime 3) which weaken in relation to changes in intensity of equatorial low-pressure zone and Tasman high. Finally, while the overall precipitation decreases in the future, regime 1 exhibits a precipitation increase resulting from the orographic enhancement of a slight increase in moisture convergence in the vicinity of New Caledonia due to the rotation of the wind flow perpendicular to the relief associated to large scale modifications.

4.3 Precipitation extremes

Extreme precipitation is expected to intensify with global warming (Collins et al. 2013). We investigate in this section
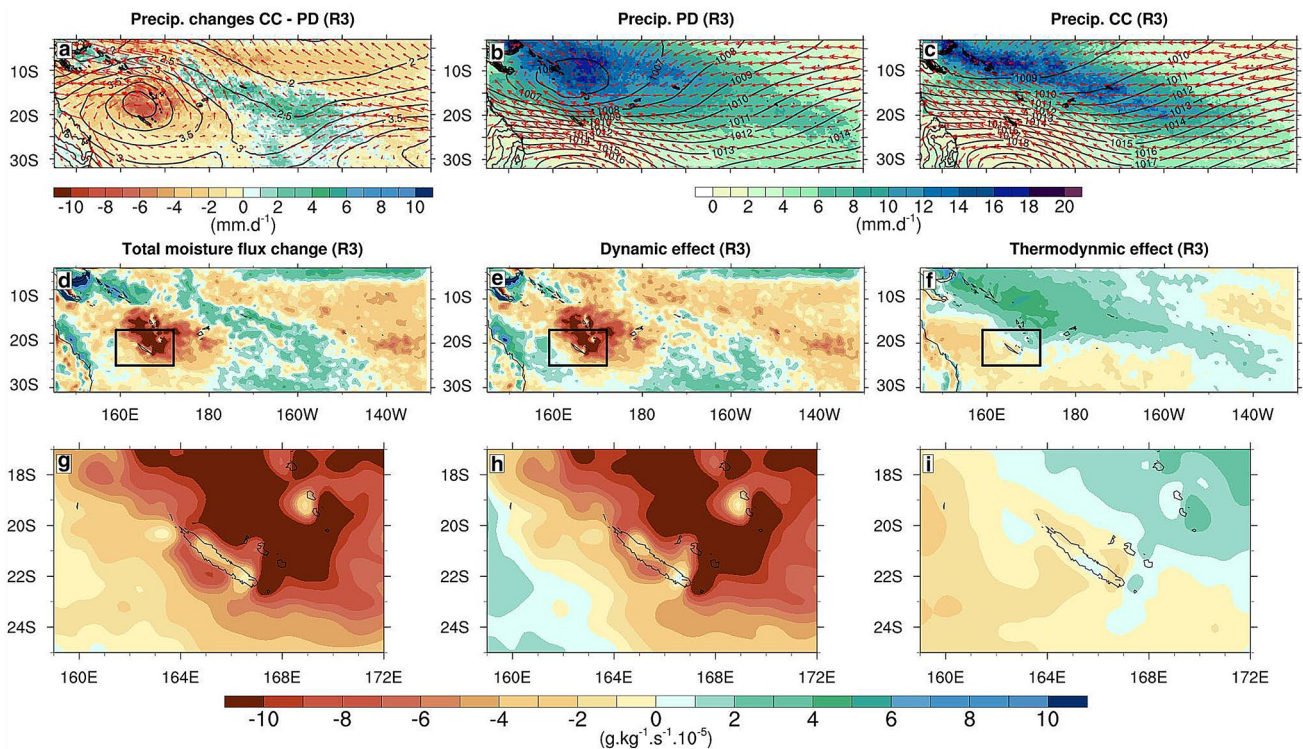
Fig. 11 Same as Fig. 10 but for regime 3

the projected changes in extreme precipitation locally over NC as well as their potential impacts on mean rainfall through the contribution of extreme events to total annual rainfall.

In present-day conditions, the spatial distribution of SDII (Fig. 12d), which represents the average amount of rainfall from rainy days, is similar to that of climatological rainfall (from all days), highlighting again the strong contrast between eastern and western NC. Extreme events bringing more than 30 mm in a day (R30mm; Fig. 12a) and the total annual precipitation from very heavy rain days (R99p; Fig. 12j) have a similar spatial distribution, with maxima located over the mountain range and an east/west contrast. The spatial distribution of the contribution of extreme events to total rainfall R99PTOT is slightly different: it is largest over the valleys near the central mountain range (Fig. 12g), and without clear east/west contrast.

Under future conditions R30mm and SDII decrease (Fig. 12c, f), while keeping relatively similar spatial organizations compared to the present-climate (Fig. 12a, d vs b, e). In CC, NC-averaged R30mm is -19% lower than in PD (3.9 days less than the 20.7 days in PD) while SDII decreases by 5% (− 0.9 mm.day^{-1} difference to 21 mm.day^{-1} in PD). The largest decrease occurs in the southern part of the mainland (Fig. 12c, f). For R99PTOT, our climate change simulation indicates that this spatial contribution will be

considerably altered by anthropogenic forcing (Fig. 12g, h): the contribution of extreme events to total rainfall considerably increases on the east coast (~ + 5% annually which is a ~ 50% increase compared to the value in PD of ~ 10%) but decreases on the west coast (~ − 3% which is a ~ 30% decrease compared to the value in PD of ~ 10%). These spatially contrasted changes result in a shift of the maximum contribution of extreme to total rainfall from the central mountain range in the present climate to the eastern coast in the future (Fig. 12g, h, i). This increase of R99PTOT over the east coast in a drying context combined with a decrease of extreme events frequency (R30mm) reveal an increase in extreme precipitation intensity. The R99P index displays a similar spatial organization in PD and CC, with a marked east/west contrast and maxima located over the mountain range, but the CC simulation exhibits also an overall 18% decrease with an amplification of east/west contrast (~ + 150 mm in the east coast and ~ -100 mm in the west coast).

In summary, the frequency of extreme rainfall events is projected to decrease over NC, in particular in southern main island, the mean precipitation intensity shows a general drying over NC, expect in the extreme north and over the loyalty islands. The spatial pattern of the contribution of extreme events to total rainfall is considerably modified with an increase on the east coast and a decrease on the west coast.
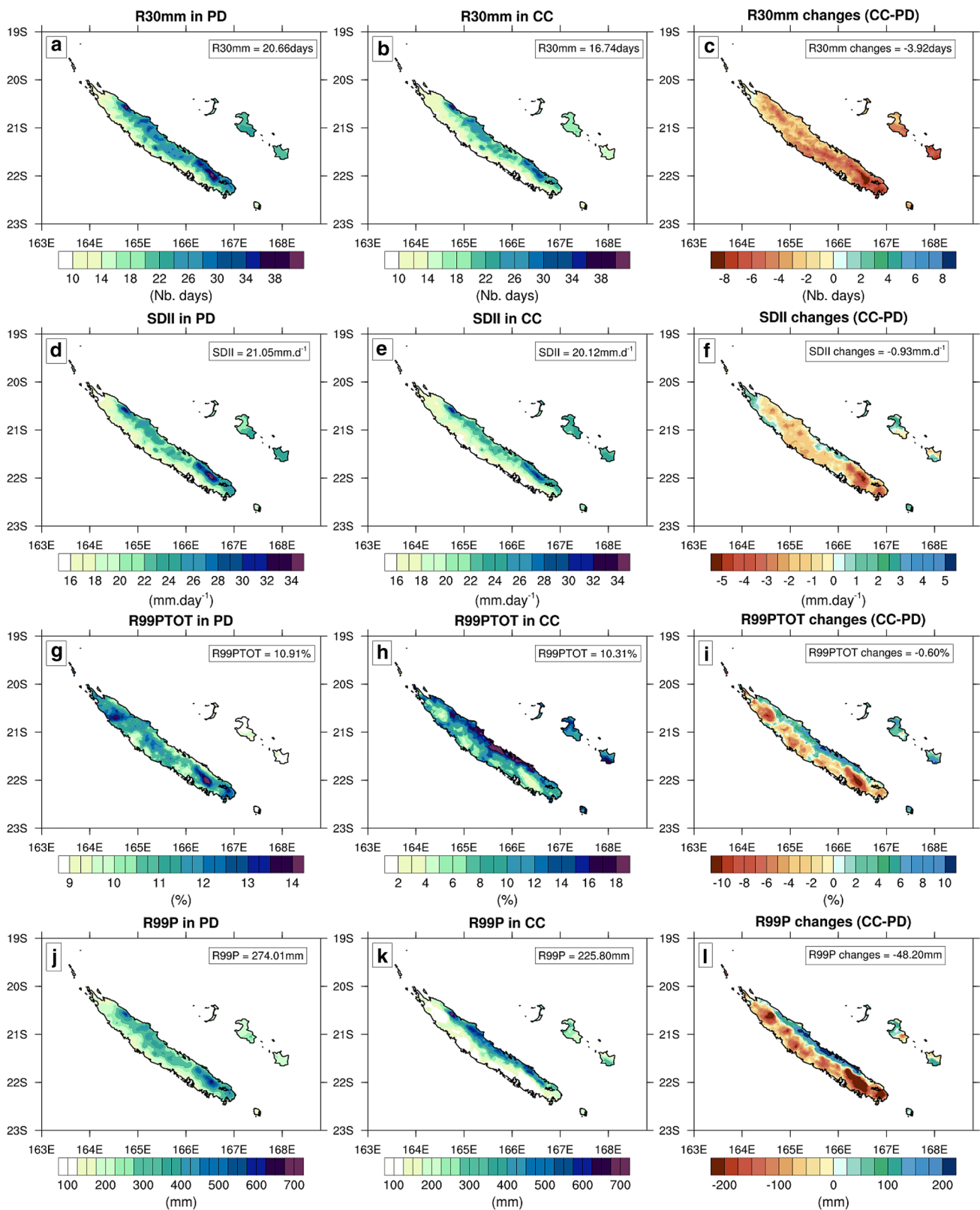
Fig. 12 First row: Annual mean of R30mm indice (in number of days) from the (**a**) PD simulation, (**b**) CC simulation, and (**c**) difference between the CC and PD simulation. Second row: Idem for SDII indice (in mm.day^{-1}). Third row: Idem for R99PTOT indice (in %). Fourth row: Idem for R99P indice (inmm). The values of area-average indices over NC are indicated in the top right-hand boxes

Hence, over eastern NC, our simulations indicate a reduction in averaged rainfall from rainy days and the number of extreme events along with an increase in the contribution of extreme precipitation to annual total precipitation, highlighting an increase in the amount of rainfall falling during extreme events compared to the climatology under future conditions.

5 Summary and discussion

This study is to our knowledge the first attempt to assess the projected precipitation changes over NC at the end of the twenty-first century. These projections were performed in the unmitigated RCP8.5 scenario, using a dynamical downscaling based on a regional atmospheric model (WRF) with a nested grid at 4 km resolution over New Caledonia. We showed that the 4 km resolution allowed resolving the main orographic features of this mountainous island and to study and understand the very spatially contrasted rainfall distribution in NC.

We also applied a two-step bias correction method to the CMIP5 multi-model mean projections used to force our model at its surface and lateral boundaries. Our bias correction strategy first removed issues associated with CMIP5 present-day biases, by adding the CMIP5 ensemble mean projected changes in lateral and surface boundary conditions to present-day estimates obtained from an atmospheric re-analysis. This is the so-called "pseudo global warming" approach. Second, we then applied an emergent constraint method (Li et al. 2016) to reduce biases in the projected CMIP5 ensemble-mean SST changes, on the basis of their statistical relations with the present-day dry western equatorial Pacific biases.

The present-day precipitation characteristics (mean state including the anchoring of precipitation maxima over orography, seasonal variability, rainfall extremes) in our present-day simulations agree reasonably with observations, much better than at 20 km resolution (see discussion in the the following and Fig. 14). This indicates that our model configuration is a reasonable tool to perform rainfall projections for NC, and that a ~ 4 km resolution is necessary to account for the strong effects of land-sea contrasts and topography on rainfall over the archipelago. The ensemble mean of the low-resolution (~ 100–200 km) CMIP5 models yields an insignificant rainfall change over NC. In contrast, our simulations yield an average 18% precipitation decrease by 2080–2100 in NC under the unmitigated RC8.5 scenario. This drying is strongest on the leeward (western) side and southern part of the mainland, and seasonally modulated, with the warm summer (NDJFMA) season representing 80% of the total rainfall decrease. The strongest drying of − 30% (and up to -45% during the hot season) is located near Nouméa.

A classification of the warm season weather regimes yielded four dominant weather regimes that are consistent with previous studies (Leroy 2006; Lefèvre et al. 2010; Specq et al. 2019). Regime 3, which corresponds to a strong trade winds regime, accounted for 83% of the NDJFMA precipitation decrease but without changes in wind direction, suggesting a dominance of changes in the synoptic circulation associated to large-scale moisture convergence rather that of local effects induced by orography. In the future climate we showed that a high-pressure anomaly around New Caledonia associated to a strong air subsidence yielded a reduced moisture convergence in the boundary layer resulting in reduced rainfall over the archipelago. More generally, the decomposition of the boundary layer moisture flux convergence showed that dynamical effects of these circulation changes dominated the thermodynamical effects associated with planetary boundary layer moistening, and therefore accounted for most of the precipitation changes in all weather regimes. There was only 1 regime exhibiting an increased precipitation (overall dominated by reduced precipitation in the future), that could be related to a slight increase moisture convergence to New Caledonia strongly enhanced by orographic effects along mountain due to a rotation of the wind flow from north-west to north-east direction (perpendicular to the relief) in the future climate.

Extreme rainfall events also become about 20% less frequent and intense in our projections. Their contribution to total precipitations (an important parameter for planning water storage) increases by ~ 50% on the windward side and decreases by ~ 30% on the leeward side of the mainland in the future. The strong increase of the contribution of the extreme rainfall events to total precipitation over the east coast is due to much stronger (+ 150 mm) projected extreme precipitation events there even though the total precipitation decreases in the future. The east coast therefore concentrates negative impacts of the hydrological cycle future changes, with a mean drying but very strong episodic precipitation events, which cause damage and make water storage more difficult.

Our results have been obtained with regional climate projections using a pseudo-global warming method, which allows removing the effect of systematic present-day biases at the domain boundaries in CMIP models. This methodology has been widely used to investigate changes in precipitation and hydrological cycle in response to climate change in various regions of the world (e.g. Ban et al. 2015; Kendon et al. 2014; Rasmussen et al. 2014; Zhang et al. 2016b). In addition to addressing present-day biases in CMIP, an original aspect of our work is the correction of biases in CMIP projected SST changes using the "emergent constraint" method of Li et al. (2016). To assess the influence of this projected SST bias correction, we also performed a climate-change simulation forced by the uncorrected projected

CMIP5 SST changes (NOTCOR in the following). As shown on Fig. 13, the NOTCOR simulation also simulates a significant drying over NC, with a similar spatial pattern to that in CC. The projected change is however stronger in NOTCOR (− 25% vs − 18% in CC). These results indicate that correcting for the projected SST change bias does not qualitatively modify the precipitation projections over New Caledonia. In contrast, Dutheil et al. (2020) show that South Pacific projected Tropical Cyclone activity changes area strongly sensitive to the SST changes, with a clear reduction when the projected SST change is corrected that does not materialize without correction. In that case, the drastic changes described in Dutheil et al. (2019, 2020) on the SPCZ drying and cyclone activity is not as striking and that may be due to the remote situation of NC which lies on the edges of the SPCZ influence. However, we hypothesize that for other islands that lie nearer the SPCZ centre of action, implementing such downscaling strategy with corrections will be important.

We relied on dynamical donwscaling to be able to resolve the interaction with large-scale circulation changes and the fine-scale topography of the mountainous New Caledonian mainland. This raises the question of what resolution is appropriate to simulate New Caledonian precipitation accurately? Our modelling strategy allows comparing the 20 km resolution of the outer domain with the 4 km-resolution nested grid over NC (Fig. 14). A 20 km resolution does not resolve the main NC orographic features adequately, much less than at 4 km resolution (dash line in Fig. 1d). Although a 20-km resolution allows simulating some aspects of present day rainfall east–west contrast, this contrast is far less pronounced than at 4 km resolution (Fig. 14a, b) and in observed estimates (Fig. 3a). The projected precipitation changes are also considerably weaker and more spatially uniform than at 4 km resolution (Fig. 14 c, d). Note that the differences discussed above may not only arise from horizontal resolution as the parameterization of subgrid-scale convection is disabled in the 4 km-resolution domain. Along the same lines, Zhang et al. (2016a) indicate that using a finer spatial resolution (1 km vs 3 km) further improves the representation of rainfall over the Hawaiian islands, which also host a marked orography. This raises the question of what resolution is appropriate to simulate New Caledonian precipitation even more accurately. Additional simulations at higher resolution will be needed to address that question.

Although the spatial resolution has a crucial importance in simulating rainfall over NC, other improvements are possible. First, the specific NC land and vegetation are not accounted for in our WRF configuration. The soil composition we used in WRF is dominated by clays, while NC has other very diverse types of soil (e.g. limestone, basalt, peridotite; Bonvallot et al. 2012). A better representation of the soil and vegetation may change the surface heat and water budgets, and thus improve the simulated rainfall. That should be investigated. More importantly perhaps, we were not in a position to test the sensitivity of the projected rainfall changes to the physical parameterizations used in the atmospheric model due to computational limitations, such as cloud microphysical schemes. Another caveat is that our study does not account for air-sea coupling. The lagoon that surrounds NC is the largest in the world (~ 20 km wide in many parts around New Caledonia) with an average ~ 20 m depth. The sea surface temperature in the lagoon will respond to climate change differently from the surrounding open sea, modifying the land-sea temperature gradient and the local low-level atmospheric circulation through sea breeze effect and frontal genesis at the lagoon/open ocean borders. Only a fine-resolution ocean–atmosphere coupled model would be able to resolve these effects and assess their potential influence.

Finally, the present-day NC rainfall interannual variability is strongly related to ENSO (Fischer 2004; Moron et al. 2016; Nicet and Delcroix 2000). Several studies (e.g. Cai et al. 2012, 2018) suggest more frequent extreme El Niños

Fig. 13 Annual mean of precipitation changes (in mm.day^{-1}) between (**a**) CC and PD and (**b**) NOTCOR and PD. The relative area-average precipitation changes over NC are indicated in the top right-hand boxes
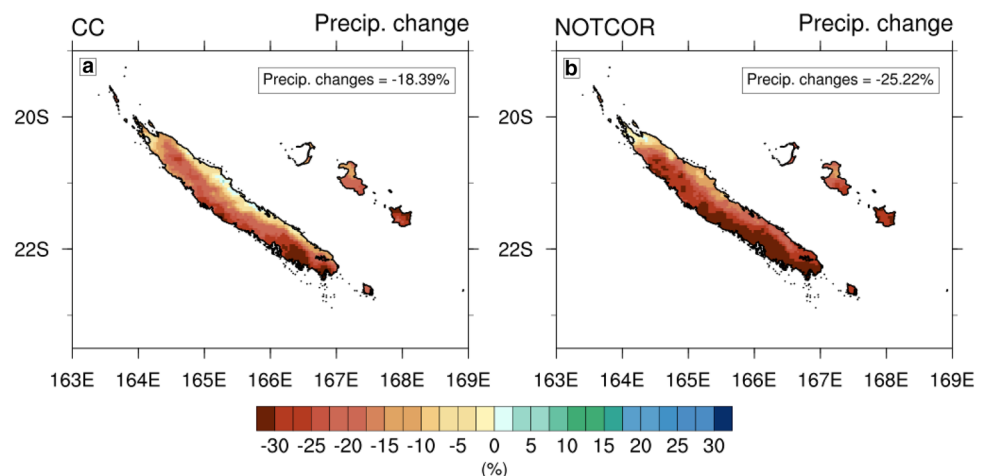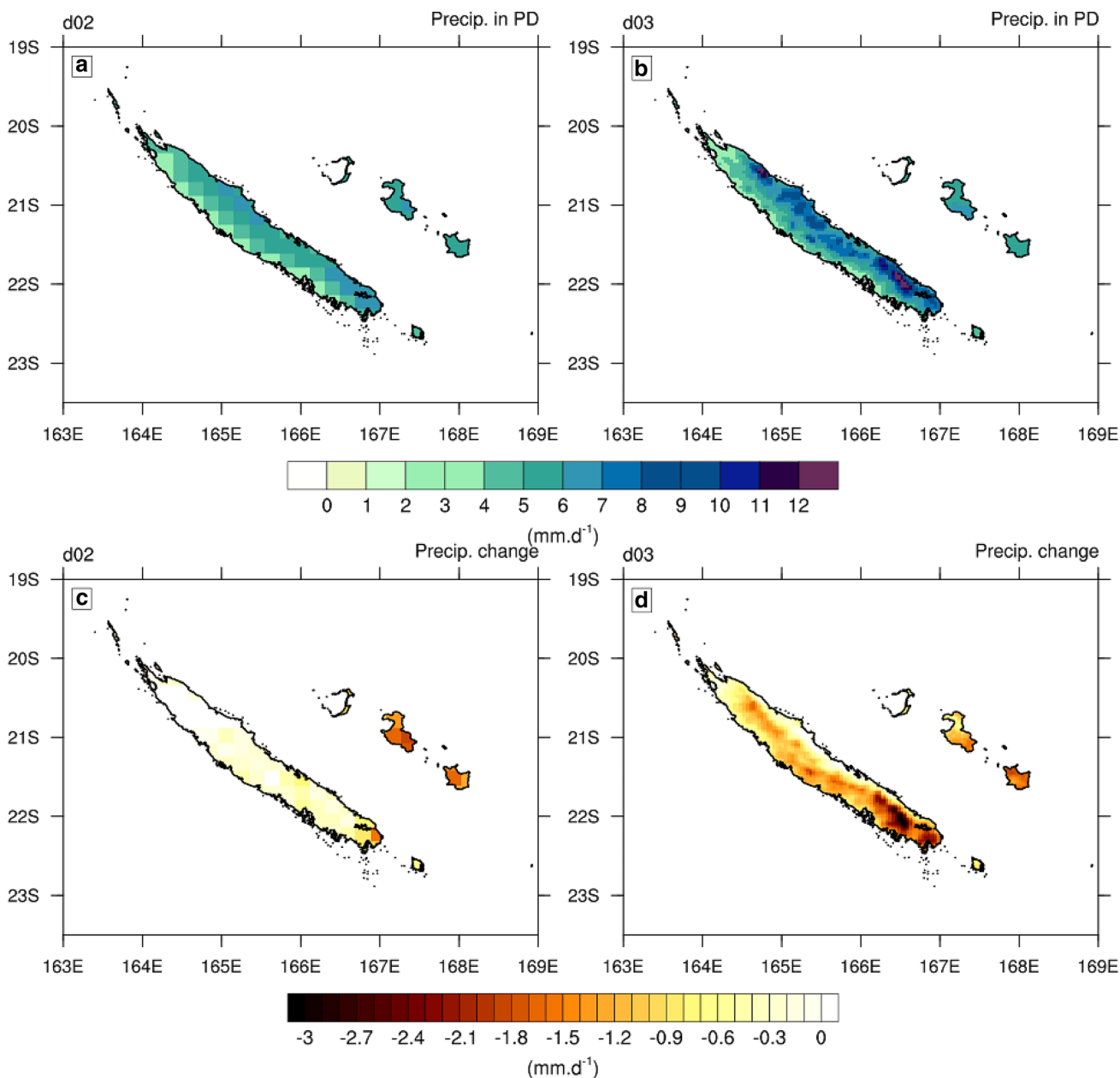
Fig. 14 Annual mean of precipitation (in mm.day^{-1}) from the PD simulation in (**a**) d02 domain at 20 km horizontal resolution and, (**b**) d03 domain at 4 km horizontal resolution. Annual mean of precipita- tion change (in mm.day^{-1}) between CC and PD in (**c**) d02 domain at 20 km horizontal resolution and, (**d**) d03 domain at 4 km horizontal resolution

and a stronger impact of ENSO on rainfall in the future climate. Our current framework does not account for changes in ENSO variability of the climate system, ENSO variability being the same in PD to CC simulations. Although changes in future ENSO variability remain uncertain (Timmermann et al. 2018), research is needed to assess how changes in ENSO may influence NC rainfall in a warming world.

The changing NC climate will not only influence rainfall and water resource, but will have wider impacts on the health, environment, economy, and energy production. For instance, NC is subject to recurrent dengue and leptospirosis outbreaks, which have themselves been linked to environmental factors such as relative humidity and maximum temperatures in NC (Descloux et al. 2012; Teurlai et al. 2015) or rainfall for leptospirosis (Tubiana et al. 2013). Our projections indicate an increase in relative humidity (+4%) combined with a strong increase in temperature (+3 °C), which could significantly increase the probability of a dengue epidemic in the future. Our projections indicate an~20% increase in surface winds, which (together with drying) will

increase risks of fire in the future climate. In summary, our projections indicate a ~ 20% drying over NC by 2080–2100. This drying could have disastrous consequences for New Caledonian water resource and ecosystem conservation, as well as for a number of other areas (public health, fire risks, etc..). It is therefore crucial that public policies carefully prepare adaptation plans to face these possible future changes.

Compliance with ethical standards

Conflict of interests The authors declare no competing interests.

References

Baltzer F, Trescases JJ (1971) Erosion, transport et sédimentation liés aux cyclones tropicaux dans les massifs d'ultrabasites de Nouvelle-Calédonie. Cahiers ORSTOM Série Géol III 2:221–244

Ban N, Schmidli J, Schär C (2015) Heavy precipitation in a changing climate: Does short-term summer precipitation increase faster? Geophys Res Lett 42:1165–1172

Benichou P, Le Breton O (1987) AURELHY : une méthode d'Analyse (Utilisant le RELief pour les besoins de L'HYdrométéorologie. (Montpellier: ORSTOM), pp 299–304.

Bonvallot J, Gay J-C, Habert É (2012) Atlas de la Nouvelle-Calédonie. IRD Editions, Marseille

Bracegirdle TJ, Stephenson DB (2013) On the robustness of emergent constraints used in multimodel climate change projections of arctic warming. J Clim 26:669–678

Bretherton CS, Park S (2009) A new moist turbulence parameterization in the community atmosphere model. J Clim 22:3422–3448

Brodribb TJ, Feild TS (2000) Stem hydraulic supply is linked to leaf photosynthetic capacity: evidence from New Caledonian and Tasmanian rainforests. Plant Cell Environ 23:1381–1388

Brown JN, Langlais C, Sen Gupta A (2015) Projected sea surface temperature changes in the equatorial Pacific relative to the Warm Pool edge. Deep Sea Res Part II 113:47–58

Brown JR, Moise AF, Colman RA (2013) The South pacific convergence zone in CMIP5 simulations of historical and future climate. Clim Dyn 41:2179–2197

Cai W, Lengaigne M, Borlace S, Collins M, Cowan T, McPhaden MJ, Timmermann A, Power S, Brown J, Menkes C et al (2012) More extreme swings of the South Pacific convergence zone due to greenhouse warming. Nature 488:365–369

Cai W, Wang G, Dewitte B, Wu L, Santoso A, Takahashi K, Yang Y, Carréric A, McPhaden MJ (2018) Increased variability of eastern Pacific El Niño under greenhouse warming. Nature 564:201–206

Cavarero V, Peltier A, Aubail X, Leroy A, Dubuisson B, Jourdain S, Ganachaud A, Gibelin A-L, Lefèvre J, Menkes C et al. (2012) Les évolutions passées et futures du climat de la Nouvelle-Calédonie.

Ceccarelli DM, McKinnon AD, Andréfouët S, Allain V, Young J, Gledhill DC, Flynn A, Bax NJ, Beaman R, Borsa P, et al. (2013) Menkes CL, The Coral Sea. In Advances in marine biology, Elsevier, pp 213–290.

Charrad M, Ghazzali N, Boiteau V, Niknafs A (2014) NbClust : an R package for determining the relevant number of clusters in a data set. J Stat Soft 61

Chazeau J (1993) Research on new caledonian terrestrial fauna: achievements and prospects. Biodiversity Lett 1:123

Chen F, Dudhia J (2001) Coupling an advanced land surface-hydrology model with the Penn State–NCAR MM5 modeling system. Part i: model implementation and sensitivity. Mon Weather Rev 129:569–585

Collins M, Knutti R, Arblaster J, Dufresne J-L, Fichefet T, Friedlingstein P, Gao X, Gutowski WJ, Johns T, Krinner G et al (2013) Long-term climate change: projections, commitments and irreversibility. In: Stocker TF, Qin D, Plattner G-K, Tignor MMB, Allen SK, Boschung J, Nauels A, Xia Y, Bex V, Midgley PM (eds) Climate change 2013—the physical science basis. Cambridge University Press, Cambridge, pp 1029–1136

Collins WD, Rasch PJ, Boville BA, Hack JJ, McCaa JR, Williamson DL, Kiehl JT, Briegleb B, Bitz C, Lin S-J, et al. (2004) Description of the NCAR community atmosphere model (CAM 3.0). 226.

Diday, E. (1971) Une nouvelle méthode en classification automatique et reconnaissance des formes la méthode des nuées dynamiques. Revue de Statistique Appliquée 19–33.

Descloux E, Mangeas M, Menkes CE, Lengaigne M, Leroy A, Tehei T, Guillaumot L, Teurlai M, Gourinat A-C, Benzler J et al (2012) Climate-based models for understanding and forecasting dengue epidemics. PLoS Neglected Tropical Dis 6:e1470

Dutheil C, Bador M, Lengaigne M, Lefèvre J, Jourdain NC, Vialard J, Jullien S, Peltier A, Menkes C (2019) Impact of surface temperature biases on climate change projections of the South Pacific Convergence Zone. Clim Dyn.

Dutheil C, Lengaigne M, Bador M, Vialard J, Lefèvre J, Jourdain NC, Jullien S, Peltier A, Sultan B, Menkès C (2020) Impact of projected sea surface temperature biases on tropical cyclones projections in the South Pacific. Sci Rep 10:4838

Fischer M (2004) A non-linear statistical downscaling model: El Niño/Southern Oscillation impact on precipitation over New Caledonia. Geophys Res Lett 31:L16204

Gastineau G, Treut HL, Li L (2008) Hadley circulation changes under global warming conditions indicated by coupled climate models. Tellus A 60:863–884

Grose MR, Brown JN, Narsey S, Brown JR, Murphy BF, Langlais C, Gupta AS, Moise AF, Irving DB (2014) Assessment of the CMIP5 global climate model simulations of the western tropical Pacific climate system and comparison to CMIP3: assesment of CMIP5 climate models for the western tropical pacific. Int J Climatol 34:3382–3399

Held IM, Soden BJ (2006) Robust responses of the hydrological cycle to global warming. J Clim 19:5686–5699

Ibanez T, Hequet V, Chambrey C, Jaffré T, Birnbaum P (2017) How does forest fragmentation affect tree communities? A critical case study in the biodiversity hotspot of New Caledonia. Landscape Ecol 32:1671–1687

Jolliffe I (2011) Principal component analysis. In: M. Lovric (ed) International encyclopedia of statistical science, (Berlin, Heidelberg: Springer Berlin Heidelberg), pp 1094–1096.

Kendon EJ, Roberts NM, Fowler HJ, Roberts MJ, Chan SC, Senior CA (2014) Heavier summer downpours with climate change revealed by weather forecast resolution model. Nat Clim Change 4:570–576

Knutson TR, Sirutis JJ, Garner ST, Vecchi GA, Held IM (2008) Simulated reduction in Atlantic hurricane frequency under twenty-first-century warming conditions. Nat Geosci 1:359–364

Kuo HL (1965) On formation and intensification of tropical cyclones through latent heat release by cumulus convection. J Atmos Sci 22:40–63

Kuo HL (1974) Further studies of the parameterization of the influence of cumulus convection on large-scale flow. J Atmos Sci 31:1232–1240

Lefèvre J, Marchesiello P, Jourdain NC, Menkes C, Leroy A (2010) Weather regimes and orographic circulation around New Caledonia. Mar Pollut Bull 61:413–431

Leroy A (2006) Utilisation des Prévisions Saisonnières en Nouvelle-Calédonie.

Li G, Xie S-P (2014) Tropical biases in cmip5 multimodel ensemble: the excessive equatorial pacific cold tongue and double ITCZ problems*. J Clim 27:1765–1780

Li G, Du Y, Xu H, Ren B (2015) An intermodel approach to identify the source of excessive equatorial pacific cold tongue in cmip5 models and uncertainty in observational datasets. J Clim 28:7630–7640

Li G, Xie S-P, Du Y, Luo Y (2016) Effects of excessive equatorial cold tongue bias on the projections of tropical Pacific climate change. Part I: the warming pattern in CMIP5 multi-model ensemble. Clim Dyn 47:3817–3831

Lin G, Lin Y-L, Farley RD, Orville HD (1983) Bulk parameterization of the snow field in a cloud model. J Clim Appl Meteorol 22:1065–1092

Madden RA, Julian PR (1994) Observations of the 40–50-day tropical oscillation—a review. Mon Weather Rev 122:814–837

Maitrepierre L, Caudmont S (2007) Atlas climatique de la Nouvelle-Calédonie. Direction Interrégionale de Météo-France en Nouvelle-Calédonie et à Wallis et Futuna, Nouméa

McClean JL, Bader DC, Bryan FO, Maltrud ME, Dennis JM, Mirin AA, Jones PW, Kim YY, Ivanova DP, Vertenstein M et al (2011) A prototype two-decade fully-coupled fine-resolution CCSM simulation. Ocean Model 39:10–30

McGree S, Whan K, Jones D, Alexander LV, Imielska A, Diamond H, Ene E, Finaulahi S, Inape K, Jacklick L et al (2014) An updated assessment of trends and variability in total and extreme rainfall in the western Pacific: trends and variability in extreme rainfall in the western pacific. Int J Climatol 34:2775–2791

McGree S, Herold N, Alexander L, Schreider S, Kuleshov Y, Ene E, Finaulahi S, Inape K, Mackenzie B, Malala H et al (2019) Recent changes in mean and extreme temperature and precipitation in the Western Pacific Islands. J Climate 32:4919–4941

Moron V, Barbero R, Robertson AW (2016) Subseasonal-to-interannual variability of rainfall over New Caledonia (SW Pacific). Clim Dyn 46:2449–2468

Myers N (1988) Threatened biotas: "Hot spots" in tropical forests. Environmentalist 8:187–208

Myers N, Mittermeier RA, Mittermeier CG, da Fonseca GAB, Kent J (2000) Biodiversity hotspots for conservation priorities. Nature 403:853–858

Nicet JB, Delcroix T (2000) ENSO-related precipitation changes in New Caledonia. Southwestern Tropical Pacific 1969–98(128):3000–3006

Payri CE, Allain V, Aucan J, David C, David V, Dutheil C, Loubersac L, Menkes C, Pelletier B, Pestana G et al. (2019) New Caledonia. In: World Seas: An Environmental Evaluation, (Elsevier), pp 593–618.

Pouteau R, Trueba S, Feild TS, Isnard S (2015) New Caledonia: a Pleistocene refugium for rain forest lineages of relict angiosperms. J Biogeogr 42:2062–2077

Power S, Casey T, Folland C, Colman A, Mehta V (1999) Inter-decadal modulation of the impact of ENSO on Australia. Clim Dyn 15:319–324

Rasmussen R, Ikeda K, Liu C, Gochis D, Clark M, Dai A, Gutmann E, Dudhia J, Chen F, Barlage M et al (2014) Climate change impacts on the water balance of the Colorado Headwaters: high-resolution regional climate model simulations. J Hydrometeorol 15:1091–1116

Small RJ, Bacmeister J, Bailey D, Baker A, Bishop S, Bryan F, Caron J, Dennis J, Gent P, Hsu H et al (2014) A new synoptic scale resolving global climate simulation using the community earth system model. J Adv Modeling Earth Syst 6:1065–1094

Specq D, Bellon G, Peltier A, Lefévre J, Menkes C (2019) Influence of subseasonal variability on the diurnal cycle of precipitation on a mountainous island: the case of New Caledonia. Mon Wea Rev MWR-D-19-0177.1.

Taylor KE, Stouffer RJ, Meehl GA (2012) An overview of CMIP5 and the experiment design. Bull Am Meteor Soc 93:485–498

Teurlai M, Menkès CE, Cavarero V, Degallier N, Descloux E, Grangeon J-P, Guillaumot L, Libourel T, Lucio PS, Mathieu-Daudé F et al (2015) Socio-economic and climate factors associated with dengue fever spatial heterogeneity: a worked example in New Caledonia. PLoS Negl Trop Dis 9:e0004211

Timmermann A, An S-I, Kug J-S, Jin F-F, Cai W, Capotondi A, Cobb K, Lengaigne M, McPhaden MJ, Stuecker MF et al (2018) El Niño-southern oscillation complexity. Nature 559:535–545

Tokinaga H, Xie S-P, Deser C, Kosaka Y, Okumura YM (2012) Slowdown of the Walker circulation driven by tropical Indo-Pacific warming. Nature 491:439–443

Tubiana S, Mikulski M, Becam J, Lacassin F, Lefèvre P, Gourinat A-C, Goarant C, D'Ortenzio E (2013) Risk factors and predictors of severe leptospirosis in New Caledonia. PLOS Neglected Tropical Dis 7:e1991. https://doi.org/10.1371/journal.pntd.0001991

Vecchi GA, Soden BJ, Wittenberg AT, Held IM, Leetmaa A, Harrison MJ (2006) Weakening of tropical Pacific atmospheric circulation due to anthropogenic forcing. Nature 441:73–76

Vecchi GA, Clement A, Soden BJ (2008) Examining the tropical Pacific's response to global warming. Eos Trans Am Geophys Union 89:81–83

Widlansky MJ, Timmermann A, Stein K, McGregor S, Schneider N, England MH, Lengaigne M, Cai W (2013) Changes in South Pacific rainfall bands in a warming climate. Nat Clim Change 3:417–423

Xie P, Arkin PA (1997) Global precipitation: a 17-year monthly analysis based on gauge observations, satellite estimates, and numerical model outputs. Bull Am Meteor Soc 78:2539–2558

Xie S-P, Deser C, Vecchi GA, Collins M, Delworth TL, Hall A, Hawkins E, Johnson NC, Cassou C, Giannini A et al (2015) Towards predictive understanding of regional climate change. Nat Clim Change 5:921–930

Zhang GJ, McFarlane NA (1995) Sensitivity of climate simulations to the parameterization of cumulus convection in the Canadian climate centre general circulation model. Atmos Ocean 33:407–446

Zhang C, Wang Y, Hamilton K, Lauer A (2016a) Dynamical downscaling of the climate for the Hawaiian Islands. Part I: present day. J Clim 29:3027–3048

Zhang C, Wang Y, Hamilton K, Lauer A (2016b) Dynamical downscaling of the climate for the Hawaiian Islands. Part II: projection for the late twenty-first century. J Clim 29:8333–8354